Astrophysics Lab "A"
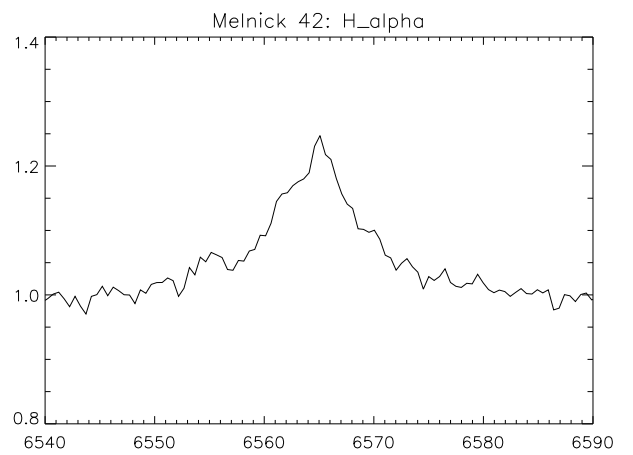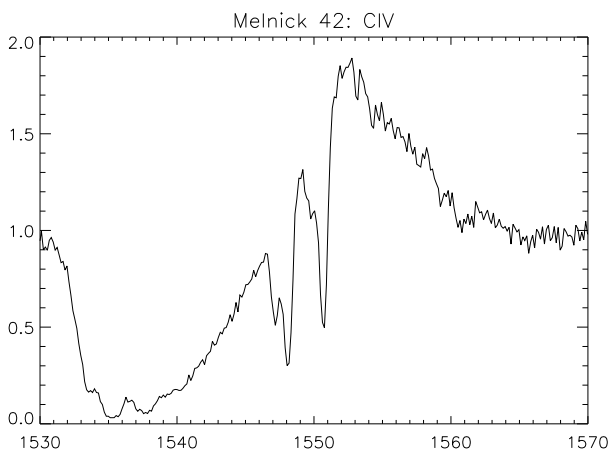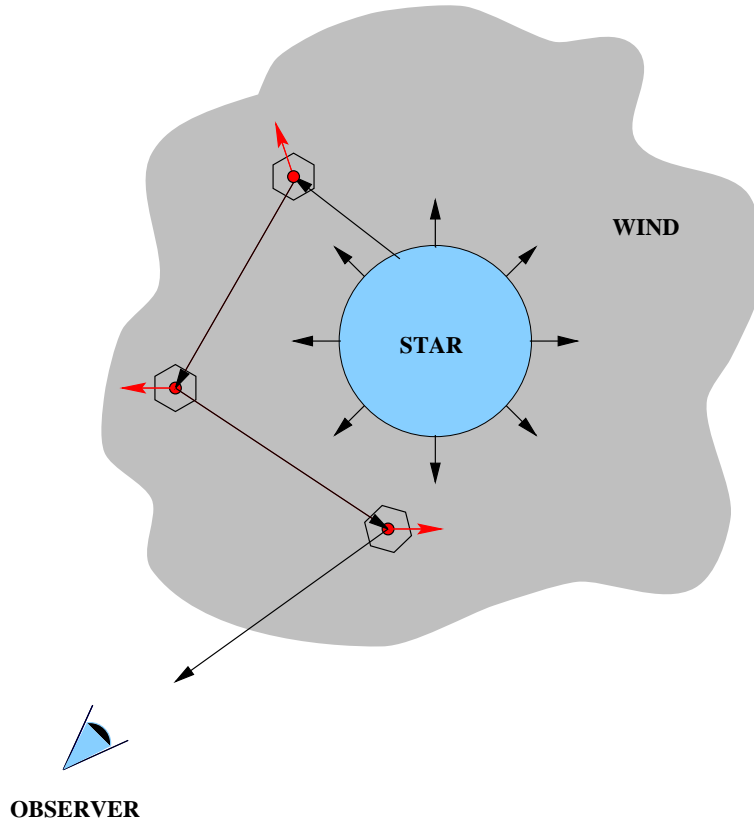
Winds from Hot Stars:

Diagnostics and Wind-Momentum Luminosity Relation

Joachim Puls (University Observatory Munich)

Melnick 42: CIV

Melnick 42: H_alpha

Contents

0 Guideline

This guideline briefly describes *what is when to do* during the preparation, implementation and elaboration of the 2-week astrophysics lab *Winds from Hot Stars: Diagnostics and Wind-Momentum Luminosity Relation (WLR)*.

- *before the first lab's afternoon:* Read carefully Sects. 1 – 6 of this manual. The content of Sect. 5 should be understood at least with respect to the basic processes. In addition, read all instructions required to carry out experiment 1 (Sect. 8.1).

- *during the first lab's afternoon:* After a discussion of the theoretical framework with the supervisor, investigate the UV-spectra of two stars (the supervisor will tell you which ones) from a sample of Galactic O-stars. In particular, determine the terminal velocities of the winds and "measure" various quantities related to the ionization of carbon and nitrogen.

- *before the second lab's afternoon:* Study Sect. 7 of this manual and prepare the implementation of experiment 2 (Sect. 8.2).

- *during the second lab's afternoon:* After discussing the results obtained on the first afternoon (plus a discussion of potential problems), carry out the H_α-analysis for the same two stars from the Galactic O-star sample. At the end of the afternoon, ask the supervisor for the UV- and H_α-data for the remaining stars of the sample.

- *after the second lab's afternoon – elaboration:* Analyze the results of your experiments and answer all related questions (Sect. 9). As a final result of this lab work, derive the WLR for Galactic O-supergiants. It is not necessary to recapitulate the content of this manual!

  Note: There are 11 questions integrated into Sections 1 to 7. Write down these questions during your preparation, since they need to be answered as well.

- Evaluation:

  It will be evaluated how well you have understood the basic theory, how far (and correctly) you have answered the questions and how well you have analyzed the outcome of your experiments.

Please do not forget: all participants have to sign for their approval of the elaboration, independent of who has done the actual work. In case a participant does not agree with certain results and no mutual consent could be achieved, (s)he is free to formulate an own answer to the given problem.

. . . and now, have fun with this lab work, which will lead us from microscopic to astronomical scales. . .

Further reading:
Kudritzki, R.-P., & Puls, J. 2000, AARev 38, 613, "Winds from Hot Stars"
Puls, J., Vink, J.S., & Najarro, F. 2008, "Mass loss from hot massive stars", A&ARv 16, issue 3, p. 209, Springer

Both reviews can be downloaded from the homepage of the supervisor.

1 Introduction

1.1 Hot, massive stars

1.1.1 Definition

Hot, luminous stars = **BRIGHT** stars. See Fig. 1.

- **hot**: effective temperature, T_{eff}, of approx.

  10,000 K ... 50,000 K (spectral type A0 - O2)

- **luminous**: 10^4 ... some 10^6 times the energy output of the sun

  For comparison: the luminosity of the sun, $L_\odot$, is

  - 3.82 * 10^{33} erg/s =
  - 3.82 * 10^{26} Watt =
  - 3.82 * 10^{20} Megawatt.

  This corresponds roughly to to the energy output from 10^{18} (one trillion) power- plants!!!

- **massive**: typical masses extend from 10 to 50 $M_\odot$. The upper mass-limit is still unknown, but should lie, for solar metallicity, well above 100 $M_\odot$.

Hot, massive stars end their lives as *core-collapse* supernovae! In the very early Universe, these stars are thought to be the major sources for the *cosmic re-ionization*.

1.1.2 Luminous stars as distance indicators

These stars are, due to their enormous brightness, visible at **large distances**.

If the energy output (luminosity) of these stars is known, the ratio

$$\frac{\text{received energy flux (at the telescope)}}{\text{radiated energy (of the star)}}$$

can be used to **determine their distances** (basically, geometric dilution of the radiation).

Thus, hot luminous stars enable us, among other things, *to determine the distances of distant galaxies to which they belong to* (at least in principal).

- With present day 10m-class telescopes (e.g., the Very Large Telescope (VLT, Paranal, Chile), the Keck-telescopes (Hawaii), the Large Binocular Telescope (LBT, Mt. Graham, Arizona), the Gran Telescopio Canarias (GTC, La Palma)), it will be possible to observe and analyze those stars up to the *Virgo cluster* in detail.

- The distance to the Virgo cluster is approx. 15 Mpc, corresponding to $\sim 5 \cdot 10^7$ lightyears (1 Mpc = $3.26 \cdot 10^6$ ly).

  For comparison:

  - the (mean) distance Earth – Sun is light*minutes*
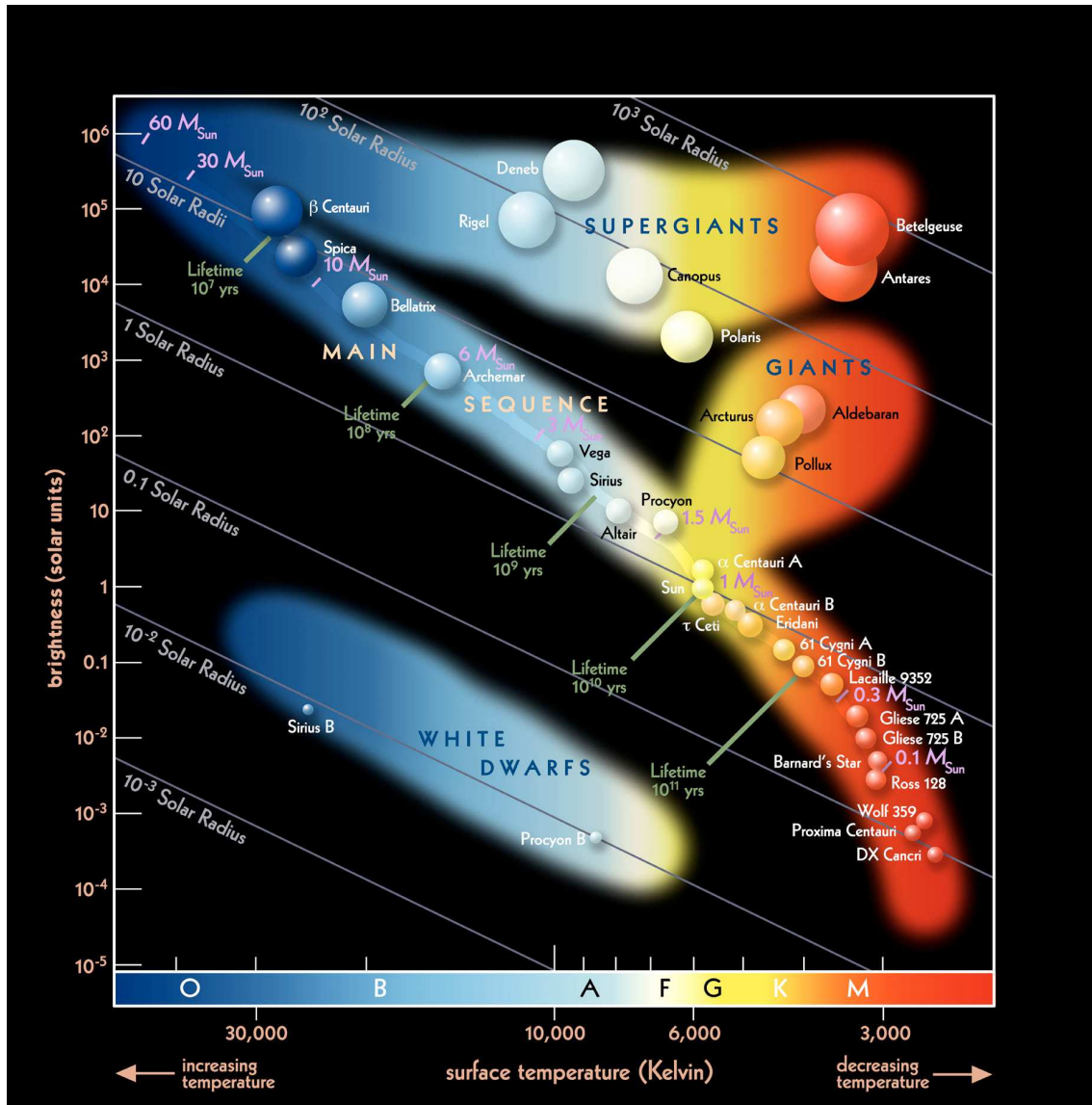
Figure 1: Hertzsprung-Russell diagram for various stellar types. Hot massive stars of spectral type O/B/A populate the "blue" region for $M \geq 10 M_\odot$ at/close to the main sequence and the uppermost "blue" supergiant regime. Indicated are (among other objects), the well-known stars Spica (= α Vir, B1 III-IV) close to the main sequence and the well-developed stars Rigel (= β Ori A, B8 Iab) and Deneb (= α Cyg, A2Iae), all of which have a significant stellar wind. Note the iso-radius contours. From "Investigating Astronomy" (http://ia.terc.edu).

- the next star, *Proxima Centauri*, lies at a distance of 4.25 ly.
- the distance between our solar system and the center of the Milky Way is approx. 27,000 ly ($\approx$ 8 kpc)
- the next neighboring galaxy of the Milky Way, the *Sagittarius Dwarf Galaxy*, lies at a distance of approx. 80,000 ly ($\approx$ 25 kpc)
- To date, successful observations of massive stars have been carried out up to distances of $\approx$ 6.7 Mpc (in NGC 3621, spiral galaxy)

- The energy flux detected by the telescopes is emitted in the outer layers of the stars, the so-called **atmospheres**.

- To calculate ("model") this radiation, a detailed description of these layers is inevitable.

- To this end, we need a **theory of stellar atmospheres**, which has been founded by *Albrecht Unsöld* in the 1930's.

1.2 Winds from hot stars

- At the end of the 1960's, the first *satellite observations* of the **ultraviolet** spectral range of stars had been performed.

- Important result: basically all hot stars with a mass larger than 15 $M_\odot$ show a high velocity outflow, the so-called

STELLAR WIND.

1.2.1 Mass-loss rate

The loss of mass per unit time suffered by the star is consequently called *mass-loss rate*, $\dot{M}$.

- Typical mass-loss rates of hot stars range from 10^{-7} to $10^{-4} M_\odot$/yr, roughly corresponding to 1/30 up to 30 earth masses per year.

- For comparison: Also the sun shows a mass outflow, the *solar wind*, though its driving mechanism is quite different from the one as discussed for hot stars below. This can already been seen from its mass-loss rate, which is significantly lower than the values mentioned above.

  $\dot{M}$ (sun): approx. $10^{-14} M_\odot$/yr (corresponding to a "Baltic Sea mass" per year or a "Great Salt Lake mass" per day).

1.2.2 Terminal velocity

Far from the stellar surface, the outflow reaches its maximum velocity. In the absence of outer forces, this velocity remains constant until large distances from the star, and thus is called *terminal velocity*, v_∞ (Newton's first *law*: "A body persists its state of rest or of uniform motion unless acted upon by an external unbalanced force.")

"Observed" data for these terminal velocities show values which are significantly higher (up to *factors of 100*) than the local speed of sound.

- Typical values for the terminal velocities lie in the range of 200 km/s (for A-supergiants) to 3000 km/s (for early O-stars).

- The speed of sound in the atmospheres of those stars varies from approx. 10 km/s to 30 km/s.

- For comparison: The terrestrial speed of sound is considerably lower, ≈ 0.3 km/s. (What is the primary origin of this difference?)

1.3 Why do we care for stellar winds?

Some points, which illustrate the astrophysical relevance of stellar winds . . .

1.3.1 Stellar evolution

Lifetime of hot stars:

- roughly 10^7 years; for comparison – lifetime of the sun: approx. $10 \cdot 10^9$ years

i.e., 1000 generations of hot stars during one generation of sun-like stars.

The **mass loss** by stellar winds (of the order of $10^{-6} M_\odot/\text{yr}$) **is significant** and amounts to $\sim 10 M_\odot$ over the star's lifetime. In other words: For a massive hot star with a typical *initial* stellar mass of 20 $M_\odot$, half of this mass is lost by stellar winds. Thus, mass loss is essential for the

STELLAR EVOLUTION

and has to be known *in all stages* of this evolution to allow for a correct description of the life and death of massive stars.

1.3.2 Galactic evolution

- Inside the stellar cores (and sometimes also in surrounding shells), energy is "created" due to *nuclear fusion*, for the largest part of the stellar lifetime by means of the CNO-cycle.

- Thus, the ratio between the elemental abundances is altered (compared to the initial ratio at the "birth" of the star).

- Thus, particularly the ratio

  hydrogen : helium : carbon : nitrogen : oxygen

  is changed.

The nuclear processed material is transported by diffusion and convection processes to the outer stellar regions, and, finally, returned to the surrounding environment by the stellar wind. Since hot stars (almost) always appear in groups ("associations"), this process can significantly change the chemical composition of the *interstellar medium* (ISM) and has therefore an important impact on the

GALACTIC EVOLUTION.

1.3.3   Star formation

- Far away from the star, the stellar wind (which is a highly **supersonic** flow) collides with surrounding matter.

- This results in the development of shocks (analog to the sonic boom) and

- in the local compression of the surrounding medium. This triggers the "birth" of new stars, i.e., affects the

<div align="center">

STAR FORMATION,

</div>

and also explains why massive stars appear mostly in associations.

1.3.4   Hot stars as distance indicators

see Sect. 1.1.2 and "wind-momentum luminosity relation"(Sect. 5.3)

1.3.5   Stellar winds as physical laboratories

- Winds of hot stars are initiated and accelerated by *radiative line driving*, also refered to as line radiation pressure[1] (compare Sect. 2. and Sect. 5).

- This process is physically extremely interesting, but cannot or only inadequately be studied in earth-bound laboratories.[2]

- By observing and carefully analyzing the emitted energy distribution of massive stars, the physics of radiative line driving can be studied in situ, i.e., we can use the stellar winds as a

<div align="center">

PHYSICAL LABORATORY.

</div>

---

[1]but note that it is not the pressure but the pressure gradient which accelerates the material.

[2]an interesting application is *laser cooling*, which exploits the radiation pressure of a laser to slow down and cool material very close to absolute zero.

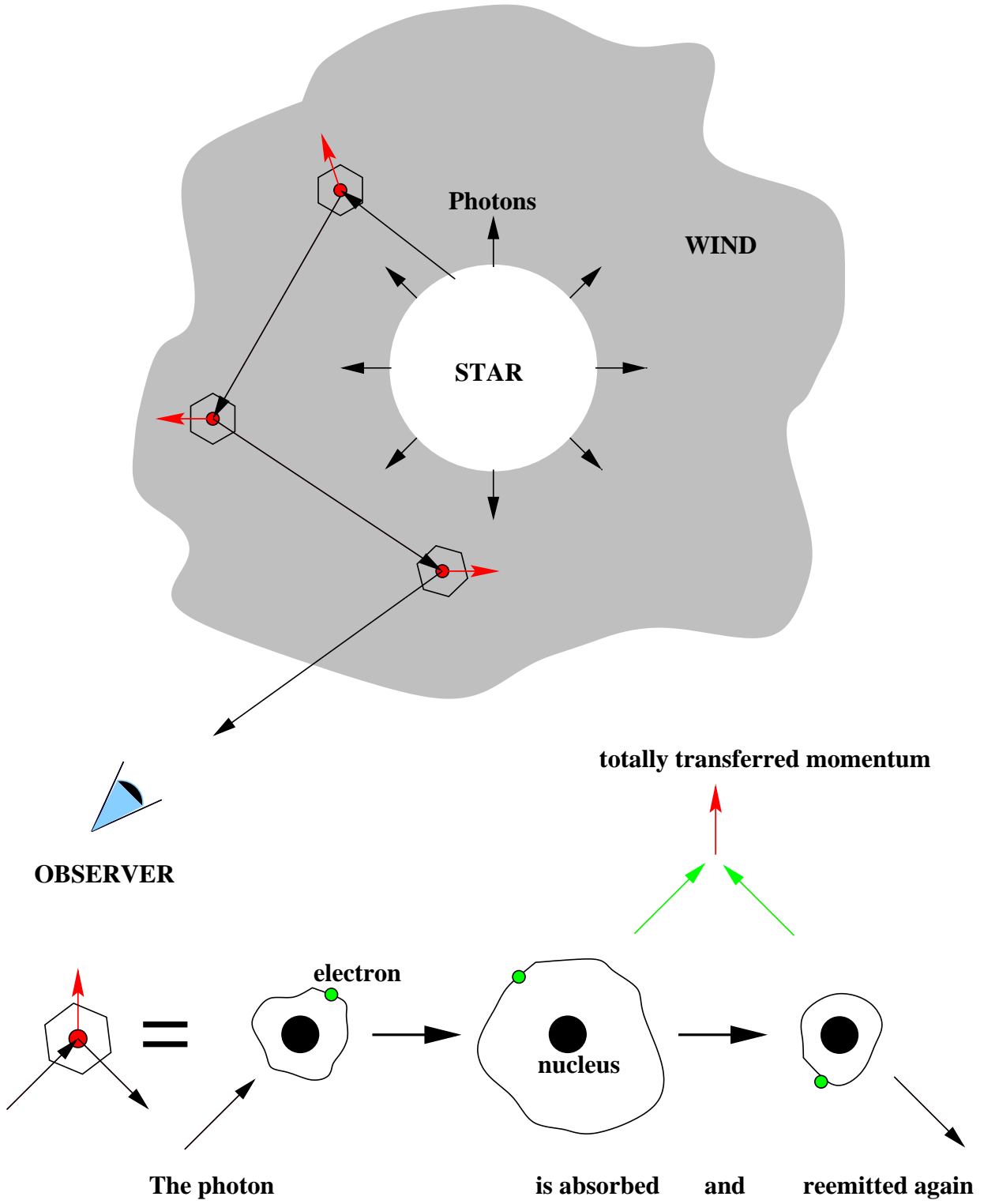# The principle of radiatively driven winds

Figure 2: Principle of radiative line-driving (see text).

2 The acceleration mechanism of line-driven stellar winds

In this section we will qualitatively describe the physical mechanism which initiates and accelerates the winds of hot stars. The corresponding formalism will be introduced in Sect. 5. The essential effects are displayed in Fig. 2.

- The deeper layers of the stellar *atmosphere*, the so-called *photosphere*, emits photons over a wide spectral range.

- During one or several interactions with the wind-material (ions), these photons transfer (part of) their *momentum* to the ions, via a two-step process (see the lower part of the figure).

  - Photons can be absorbed by an ion (e.g., carbon, nitrogen, silicon, iron, nickel etc., all of which are present in the stellar atmosphere = photosphere + wind) if their energy is equal to the energy required to excite an electron of that ion.

  - During this process not only the energy of the photon is "transformed" into excitation energy (the photon is thereby destroyed) but also momentum is transferred to the ion. Since the majority of the photons originate from the stellar "surface" (photosphere), i.e., from "inside", the ions are, on average, accelerated into the outward direction.

  - After a relatively short time, the so called mean lifetime (of the order of 10^{-8} s), the electron "falls" back to its ground state or to a different, low-energy orbit (spontaneous decay).

  - The energy lost by the electron is compensated by the emission of a "new" photon.

  - As well, the momentum of the emitted photon has to be compensated by the momentum of the emitting ion, i.e., the ion is accelerated into the opposite direction of the photon.

  - The resulting net-acceleration of the ion due to absorption and emission is the vector-sum of both accelerations.

  - Since the direction, into which the photon is emitted, is arbitrary (all directions have (almost) the same probability), the acceleration due to emission processes cancels out, when considering many such events, and only the outward directed acceleration due to absorption processes survives.

- Finally, the outward accelerated ions transfer their momenta to the bulk plasma of the wind (basically hydrogen) via Coulomb collisions, and the *total* wind is accelerated outward.

- Since the photospheric radiation field of hot stars is strong (remember that the emitted flux is $\propto T_{\mathrm{eff}}^4$) and the number of *possible* electron transitions is large, the observed mass-loss rates and terminal velocities can be easily explained. (In cooler stars, the radiation field is too weak to initialize a wind by this process, though other mechanisms can serve as accelerating agents.)

Since the above electron transitions are of bound-bound type, i.e., *line* transitions, the wind acceleration is due to

RADIATIVE LINE DRIVING.

3 UV observations of hot stars

In the following we will present typical **spectra** of hot stars taken in the UV-range. The wavelength range covers $1150 \ldots 1850$ Å.

A first series of spectra consists of observations performed with the *IUE* (International Ultraviolet Explorer) satellite, one of the most important (earlier) instruments for the wind diagnostics of hot stars, and displays Galactic objects.

A second series displays UV-spectra from typical stars in the *Small and Large Magellanic Cloud* (SMC and LMC), collected by the more recent and well-known *HST* (Hubble Space Telescope). The Magellanic Clouds are relatively small and young neighbor galaxies of our Milky Way and can be found on the southern sky.

Note: The last UV observatory launched so far was *FUSE* (Far Ultraviolet Spectroscopy Explorer), which had the highest sensitivity in the spectral range between 900 to 1200 Å (i.e., shortward from the IUE and HST range). The collected spectra gave a lot of information on ions which could not be investigated during previous missions. With respect to the spectroscopy of hot massive stars, these observations had a particular impact on the so-called clumping problem (Sect. 10).

The two series of spectra displayed here are plotted as a function of wavelength. The spectra are normalized with respect to the continuous energy distribution emitted by the photosphere, which consequently lies at "1" in the figures.

In particular, note the broad lines at

- approx. 1240 Å (N^{4+}, 4-times ionized nitrogen)

- approx. 1400 Å (Si^{3+}, 3-times ionized silicon)

- approx. 1550 Å (C^{3+}, 3-times ionized carbon)

- approx. 1720 Å (N^{3+}, 3-times ionized nitrogen)

Except for the last one, the other lines are so-called *resonance lines*, formed by transitions of the valence electron from the ground state to an excited state (often the first one) and back again. During this lab, two resonance lines from the above list, namely from 4-times ionized nitrogen (= Nv in astrophysical nomenclature) and from 3-times ionized carbon (Civ), will be analyzed.

The above lines are usually *very* broad and easily identified. They have a peculiar shape, with a blue-shifted absorption and a red-shifted emission component, called "P-Cygni profiles" (see next Sect.). Since they are formed over the *entire* wind range, they provide us with a multitude of information on the wind conditions, as will be also explained below.

The multitude of other lines which are visible in the spectra is mostly formed in the deeper wind (at lower velocities) or in the photosphere (negligible velocity), and is of minor interest in the context of the present lab.

The stars we are dealing with in the following are of *spectral type* "O", i.e., stars with surface temperatures **hotter than 30,000 K** (O3 hotter than 45,000 K).
The label(s) following the *luminosity class* (I=supergiants to V=dwarfs) serve as an identifier for certain peculiarities in the (optical!) spectra and are of no further interest here.

Let us finally address the identifiers for the individual stars. These are based on the author of the particular catalogue in which they are listed (e.g. HD = Henry Draper) plus a number

(or coordinates, as in the Sk (=Sanduleak)- catalogue), or they are numbered with respect to
the region in which they are located, as it is the case for the NGC 346-stars (sometimes, this
numbering is not unique, but depends on the specific catalogue as well).

3.1   UV spectra (IUE) of hot stars in the Galaxy

The IUE-spectra presented below have been kindly provided to us by Ian Howarth and Raman
Prinja (both University College, London). As already mentioned, mass-loss rates and terminal
velocities have to be determined during this lab, and are not quantified in the captions. The
stellar parameters quoted $(T_{\rm eff}, R_*, M_*)$ refer to values which have been derived in the 1990's
(see Table 1). Note, however, that the atmospheric models required to derive these parameters
have been significantly improved meanwhile, necessitating an update of their values. Most
importantly, the effective temperatures derived nowadays are somewhat lower than the values
presented here (by 2,000 to 5,000 K), which plays a minor role for the following investigations
though. E.g., for cooler $T_{\rm eff}$ the derived mass-loss rates need to be reduced as well (Why? Hint:
see Eq. 43), so that the WLR is hardly affected.
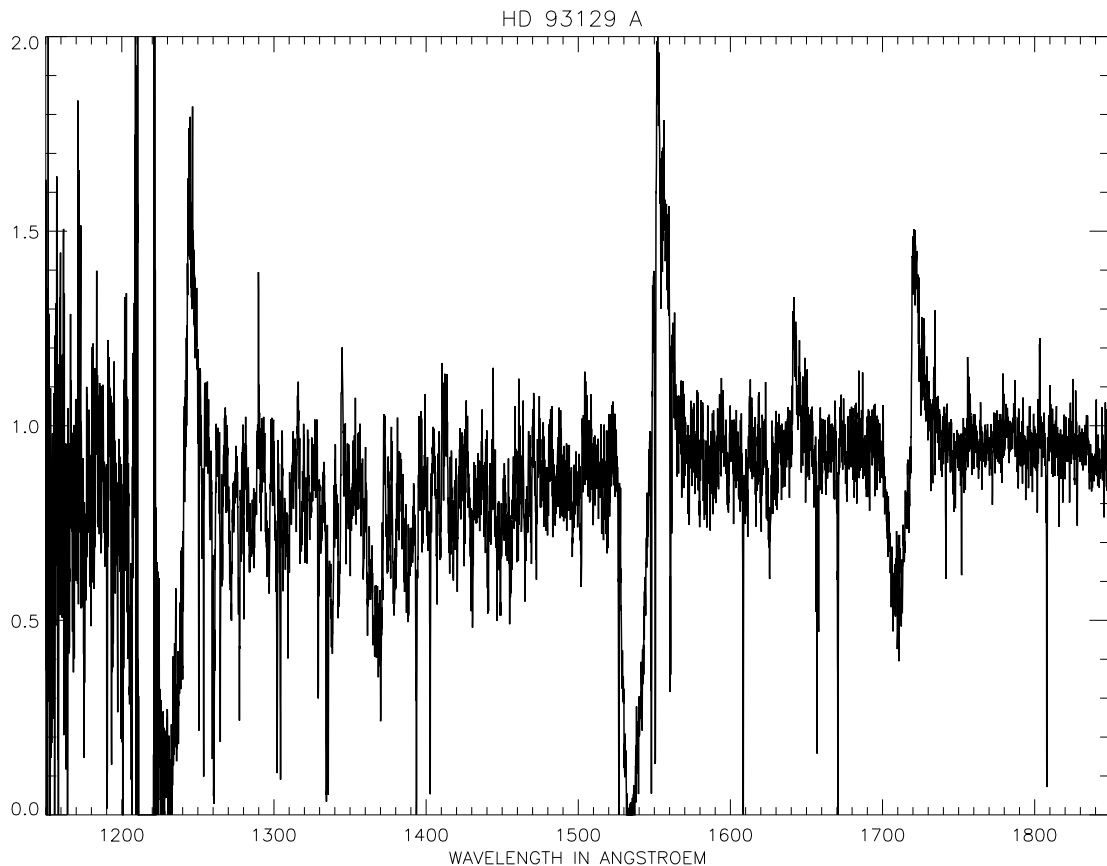
Figure 3: HD 93129A – knowledge state 1996: spectral type O3 If*, "heaviest star of the Galaxy."
$T_{\rm eff} = 50{,}500$ K, $R_* = 20\ R_\odot$, $M = 130!\ M_\odot$, $\dot{M} = ?$, $v_\infty = ?$.
To-date, this star is classified as O2 If* (the spectral class O2 has been introduced 2002), and
has been identified as a binary, consisting of two similar components with masses around 70 $M_\odot$.
As well, $T_{\rm eff}$ needed to be revised, down to 45,000 K, because of better atmospheric models.
This correction is one of the largest encountered so far (see text).
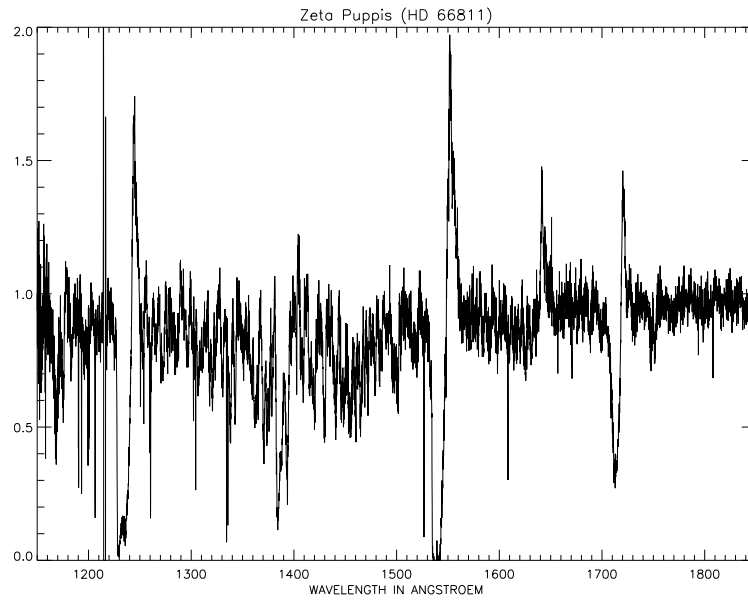
Figure 4: HD 66811 (ζ Pup) – O4 I(f): This star (southern sky) is considered as the Rosetta stone of hot star wind physics! T_{eff} (1996) = 42,000 K, $R_* = 19\ R_\odot$, $M = 53\ M_\odot$, $\dot{M} = ?$, $v_\infty = ?$. The present day value of T_{eff} is $\approx$ 40,000 K.
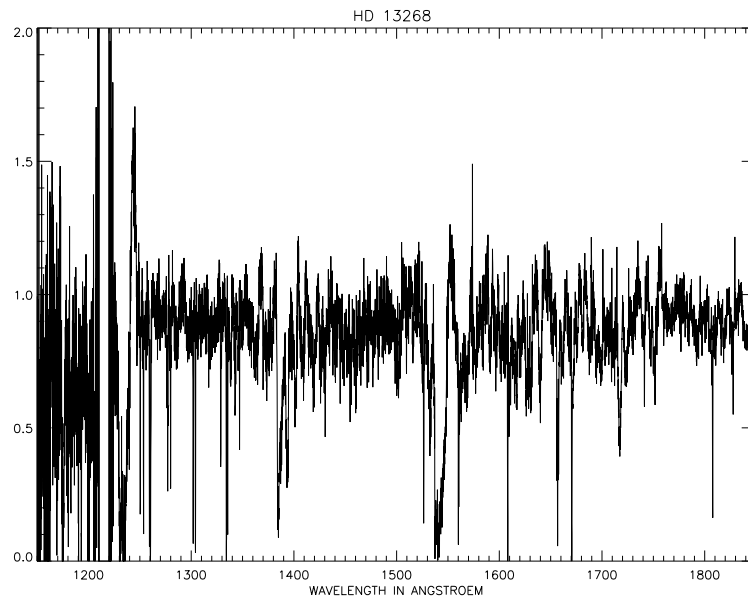
Figure 5: HD 13268 – O8 III: Rather/very low mass-loss rate! T_{eff} (1996) = 35,000 K, $R_* = 12\ R_\odot$, $M = 16\ M_\odot$, $\dot{M} = ?$, $v_\infty = ?$. The present day value of T_{eff} is 33,000 K.
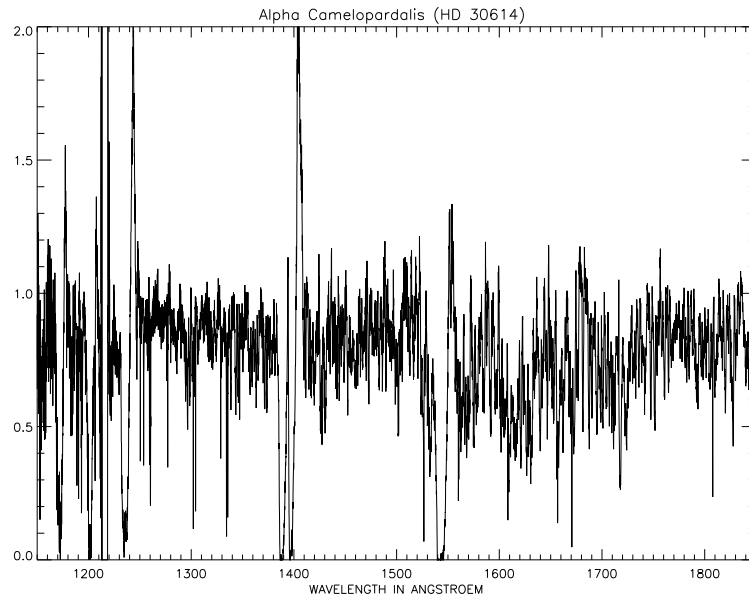
Figure 6: HD 30614 (α Cam) – O9.5 Ia: Another key object, this time on the northern sky. $T_{\text{eff}} = 30,000$ K, $R_* = 29$ $R_\odot$, $M = 31$ $M_\odot$, $\dot{M} = ?$, $v_\infty = ?$. For this star, an only marginal temperature correction by 500 K is necessary.

3.2 UV spectra (HST) of hot stars in the SMC

Note: the temperature reductions encountered for Galactic stars is much lower for SMC stars, due to the overall lower abundance of "metals" (astrophysical slang: everything except hydrogen and helium).
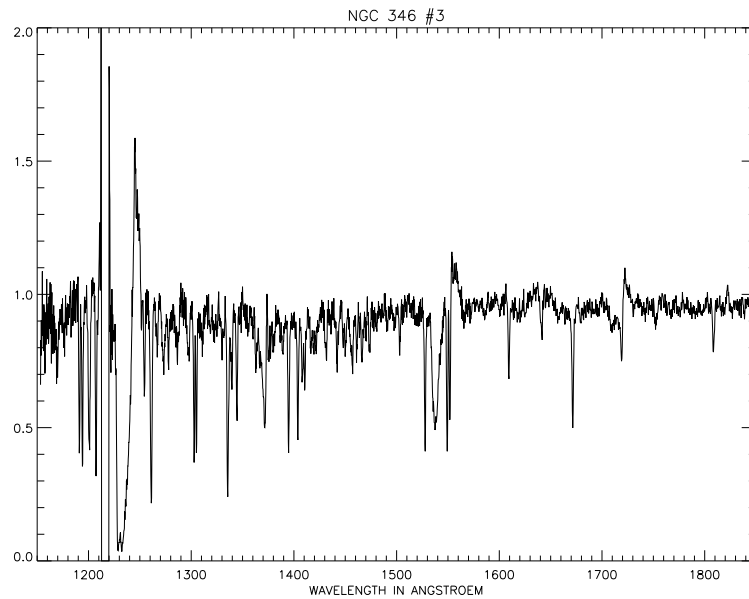
Figure 7: NGC 346 #3 (catalogue by Niemela et al. 1986) – O3 IIIf*: T_{eff} (1996) = 55,000 K, $R_* = 12$ $M_\odot$, $M = 44$ $M_\odot$, $\dot{M} = 2.3 \cdot 10^{-6} M_\odot/\text{yr}$, $v_\infty = 2900$ km/s.
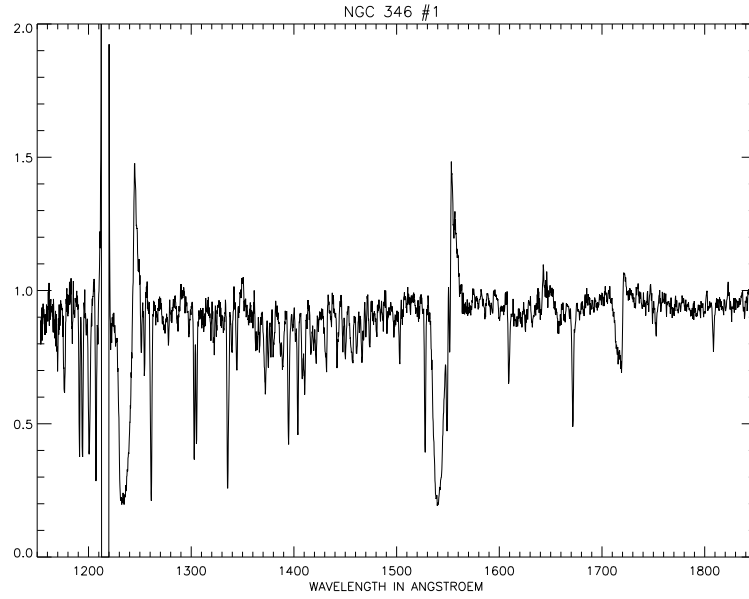
Figure 8: NGC 346 #1 (catalogue by Niemela et al. 1986) = NGC 346 #644 (catalogue by Massey et al. 1989) – O4 III(n)(f): Compare to ζ Pup! T_{eff} (1996) = 42,000 K, $R_* = 23\ R_\odot$, $M = 88\ M_\odot$, $\dot{M} = 4.8 \cdot 10^{-6} M_\odot/\mathrm{yr}$, $v_\infty = 2600$ km/s.
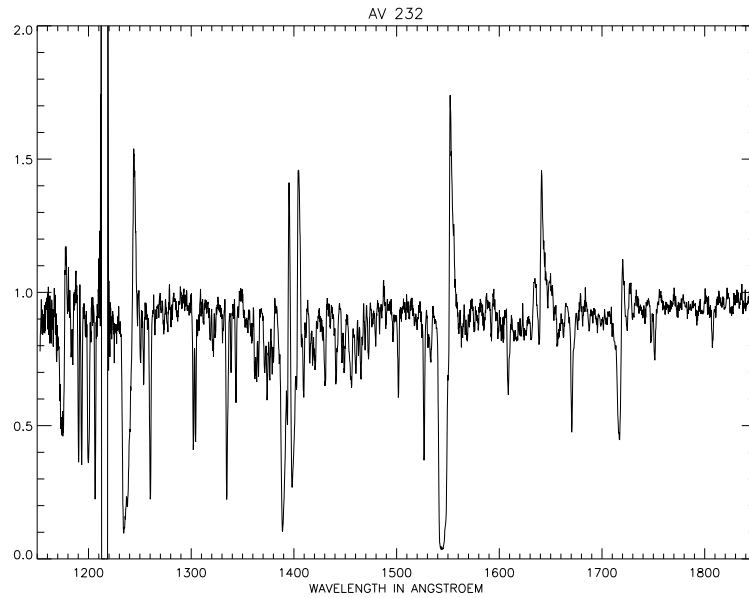
Figure 9: AV 232 = Sk 80 = NGC 346 #789 (catalogue by Massey et al. 1989) = NGC 346 #1 (catalogue by Evans et al. 2006) – O7 Iaf$^+$. T_{eff} (1996) = 37500 K, $R_* = 29\ R_\odot$, $M = 62$ $M_\odot$, $\dot{M} = 5.5 \cdot 10^{-6} M_\odot/\mathrm{yr}$, $v_\infty = 1400$ km/s. Present results indicate that this object might be a binary. Note that SMC stars have lower terminal velocities than analogue stars from the Galaxy.

3.3   UV spectra (HST) of hot stars in the LMC
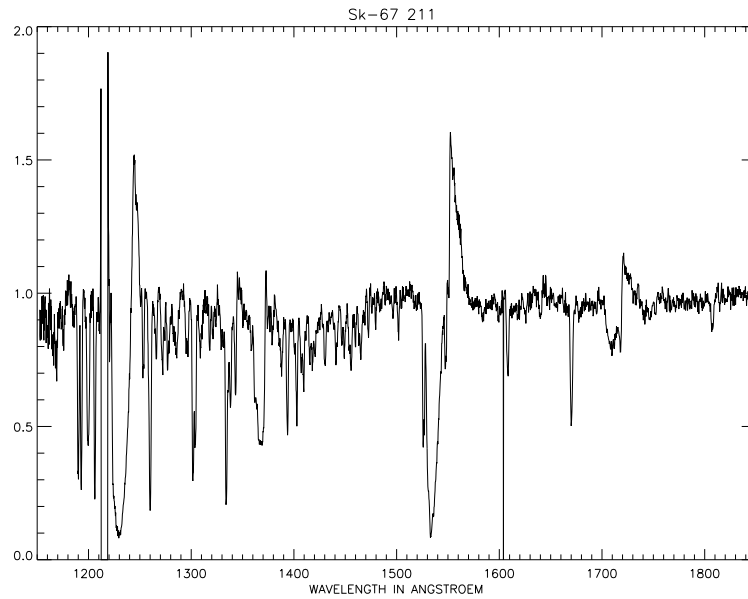
Figure 10: Sk-67 211 – O3 III(f*): T_{eff} (1996) = 60,000 K, $R_* = 18\ R_\odot$, $M = 163\ M_\odot$, $\dot{M} = 10 \cdot 10^{-6} M_\odot/\text{yr}$, $v_\infty = 3750$ km/s (velocity record!). Both the temperature and the mass are certainly too large, but this object has not been re-analyzed so far.
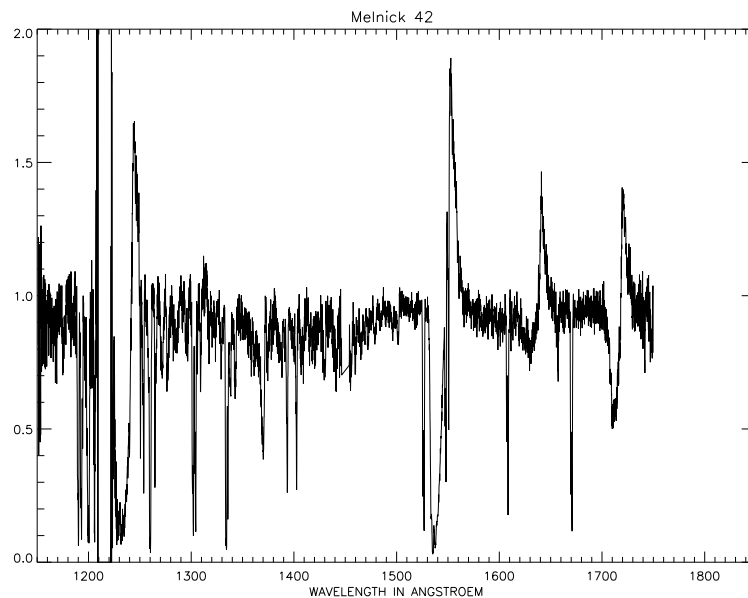
Figure 11: Melnick 42 – O3 If/WN: One of the hottest stars observed by HST in detail. T_{eff} (1996) = 50,500 K, $\dot{M} = 35 \cdot 10^{-6} M_\odot/\text{yr}$, $v_\infty = 3000$ km/s (see cover picture). The stellar radius has to be determined during this lab work! Chances are high that also here the effective temperature has been overestimated.
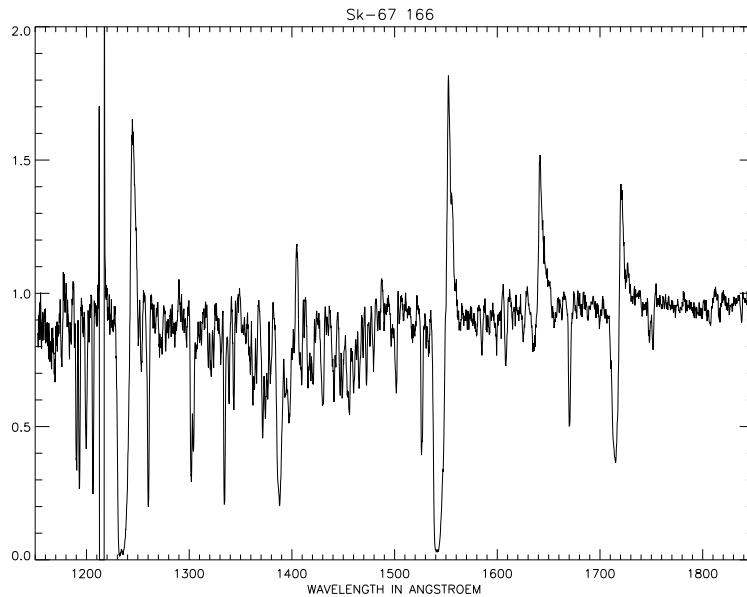
Figure 12: Sk-67 166 – O4 If$^+$: T_{eff} (1996) = 47,500 K, $R_* = 19 \ R_\odot$, $M = 62 \ M_\odot$, $\dot{M} = 13 \cdot 10^{-6} M_\odot/\text{yr}$, $v_\infty = 1900$ km/s. Two recent analyses resulted in $T_{\text{eff}} \approx 40,000$ K, similar to the effective temperature of its Galactic counterpart, ζ Pup.

4 P Cygni profiles

4.1 Formation

As mentioned above, the broad "P Cygni profiles" which are observed in the UV of hot stars allow us to investigate the physical conditions of the stellar wind in which they are formed. Their name relates to the fact that such profiles have been firstly detected in the (optical FeII) spectra of the star P Cygni.

Since the diagnostics of such profiles is a central topic of this lab, we will qualitatively illustrate how they are formed.

Note at first that the central effect is the *Doppler-effect*, which is already known from daily life.

Imagine what happens when a police car or an ambulance with turned on sirens at first approaches an "observer" at rest and then departs into the other direction. At first you will hear the siren with relatively high tones, at higher *frequencies* than the driver or if the car would be at rest. The pitch becomes instantaneously deeper at that moment when the car passes the "observer" and departs. The frequencies are now deeper than heard by the driver (who of course hears always the same frequencies).

The analogue effect[3] – now with respect to the frequency of light – is seen by an observer at rest outside the wind if he[4] observes different parts of the wind (for the following argumentation, see Fig. 13):

- If he observes the forward wind hemisphere (part A, B), he sees only approaching wind material, where its speed increases from inward to outward:

---

[3]besides certain subtleties which are due to the fact that photons propagate with the speed of light.

[4]without loss of generality, in the following we assume a male observer.

P Cygni profile formation
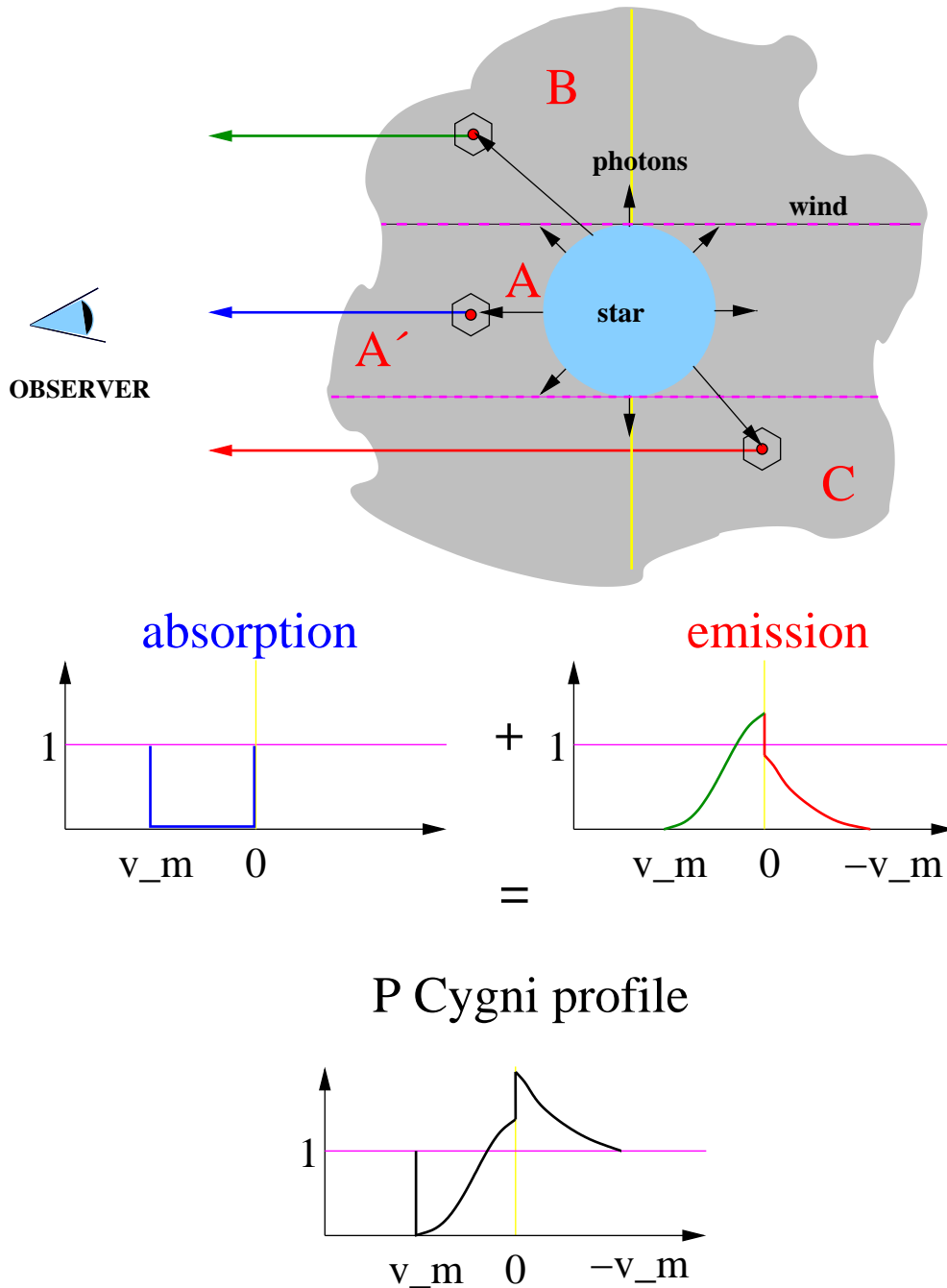
Figure 13: Formation of P Cygni profiles

- The outermost material approaches to him at highest velocities (with a maximum velocity v_∞), and he sees the radiation with a higher frequency than the the (co-moving) ions of the wind would "see" it.

- Referred to the observer, the innermost material has a velocity of almost zero, i.e., he sees the radiation at (almost) the same frequency as the wind material does.

- Looking upon the backward hemisphere (part C), the material is *departing* from the observer. Thus, the observed frequencies are lower, i.e., at larger wavelengths. Basically all velocities between zero and $-v_\infty$ can be seen, where the "minus sign" refers to the fact that the matter is moving away from the observer.

Once this argumentation has been understood, the unique shape of a P Cygni profile can be explained as follows:

- At first, let us examine the absorption processes in the wind, i.e., the *excitation* of electrons by the photospheric irradiation. Compared to the *unaffected* stellar continuum (corresponding to the line at "1"), that part of the stellar continuum will be absorbed which lies in a frequency range which can be affected by the Doppler effect due to *approaching* wind material, i.e., for frequency shifts in between zero and v_∞. (Instead of v_∞, the sketch displays the velocity v_m, which is the *m*aximum velocity at which still enough *absorbing* particles are available, with $v_m \leq v_\infty$). Absorption of radiation at highest frequencies takes place in the outermost wind, and absorption close to line center takes place in the inner one.

  Regarding the absorbing ions, the situation is vice versa: An electron transition can take place only if the photon's energy (in the atomic rest frame!) is compatible with the energy separation of the two bound states (plus/minus a small $\Delta\nu$ due to the thermal motion of the ions). Since the ions are comoving with the wind, a photon has to "start" with a *higher* rest frame frequency (compared to this transition frequency) at the photosphere to be seen *at* the transition frequency from the ion in order to be absorbed.

  Absorption processes which can be directly observed occur in part A of the wind, *in front of the stellar disk*, and result in the shown absorption profile.[5] Note the asymmetry of the absorption trough with respect to line center (zero frequency shift), since only the *approaching* wind material can absorb the stellar continuum irradiated into the observer's direction.

- On the left and right hand side of the resulting absorption trough (i.e., at Doppler shifts corresponding to velocities $\geq v_m$ and < 0), the observer sees the unattenuated stellar continuum (emitted from the stellar disk towards the observer), since there is no material present which could absorb this radiation in the corresponding frequency range.

- Because of the finite lifetime of the excited state, a new photon will be *re-emitted* after the absorption.

- Overall, an observer would see an emission profile resulting from a multitude of such processes at different velocities. Since wind emission provides *additional* radiation, the corresponding profile "starts" at zero and not at "1".

---

[5] Actually, absorption processes take place everywhere, but can be *seen* only for material in front of the disk, since only there we can compare with the stellar continuum.

- In contrast to the absorption case, however, an observer sees radiation from both hemi-spheres of the wind, i.e., from approaching and departing material. Three different regions contribute to the emission:

  - Part A' = A in front of the stellar disk, i.e., the absorbing part. Here, radiation re-emitted *into the observer's direction* is seen. Remember that emission processes are (almost) isotropic (Sect. 2), i.e., a certain fraction will be always emitted into the observer's direction.
  - Part B consisting of the forward side-lobes. The (required) excited electrons result from the absorption – not visible for the observer – of a stellar continuum that originally *did not point towards the observer*. Part A' and B form the high-frequency (left) part of the emission profile.
  - Part C consists of the backward side-lobes, i.e., material of the back hemisphere not covered by the stellar disk. Here, the radiation emitted towards the observer follows the absorption of a continuum originally directed away from the observer. Since the emitting wind material is moving away from the observer, the corresponding frequency shift is negative.
  - The overall emission profile is asymmetric, since the emitting part with positive veloc-ities (positive frequency shift) is larger than the analogue part with negative velocities (and negative frequency shifts). The figure clearly shows that the emitting "cylinder" A' *in front* of the stellar disk has no counterpart *behind* it, since the latter is covered by the star itself.
  - The reason why the emission profile has its maximum at zero and vanishes towards frequency shifts at $\pm v_m$ can be simply understood in terms of geometrical effects. The emitting areas which have the same projected[6] velocities are extremely different! The largest of these areas corresponds to a projected velocity of zero (dividing the forward and the backward side-lobes, plus the forward stellar surface), such that the emission at frequency shift zero is largest. The larger the projected wind velocity, the smaller the corresponding emitting area. Since there are no absorbing/re-emitting ions at velocities larger than $\pm v_m$, the emission profile is restricted to this velocity range.

- From the superposition of the (asymmetric) absorption and emission profiles, the typical P Cygni profile shape is readily understood.

For completeness, it remains to be said that a P Cygni line will form as described above only if enough absorbing and emitting ions are *present everywhere* in the wind. If the population is low, the profile becomes weaker, both with respect to depth and height above "1". One example of such an effect has already been considered. If there is only absorbing material present with $v_m < v_\infty$, the P Cygni profile becomes narrower compared to the maximum possible extent of $\pm v_\infty$. This and other effects which modify the profile shape will be now.

4.2   Diagnostics of P Cygni profiles

In this Section we will clarify what can be actually learned about the wind conditions when investigating P Cygni profiles. The formation mechanism as described above essentially offers *three* possibilities:

---

[6]The frequency shift due to the Doppler-effect is determined by the *projected* velocity.

- **Determination of the terminal velocity**: If there are enough absorbing ions *everywhere in the wind*, the terminal velocity can by simply determined by measuring the position of the "blue" absorption edge. All one has to do is, at least in principal, to measure the frequency of the continuum break at the "left" side of the profile and to employ the relationship between frequency shift and velocity. This is given by the simple Doppler formula

$$v_m/c = \Delta\nu/\nu_\mathrm{i}$$

  where $\Delta\nu = \nu_m - \nu_\mathrm{i}$ = frequency of the blue edge - frequency of the absorbed photon,

  and the frequency of the absorbed photon can be calculated from the energy difference between the excited and the initial state. (Which approximations have been made here?) During this lab you will become familiar with the corresponding measuring technique (and related problems).

- **Determination of the ion densities**: If the observed profile never reaches zero intensity over its whole width (such a profile is called *unsaturated*), the ionic density distribution can be determined from a comparison between synthetic and observed profiles. One "just" needs to vary the ion densities within appropriate simulations, until the resulting theoretical profile fits the observed one. This method will be tested during our lab as well. Extending this method, it is even possible – at least under favourable conditions – to determine the mass-loss rate or the elemental abundances of the contributing ions!

- **Determination of the shape of the velocity field**: Particularly when the observed profile is saturated, i.e., when the line flux reaches "zero" close to the blue edge, this shape can be determined by varying the shape of the *input* velocity field and fitting corresponding theoretical profiles to the observations. Note that different velocity fields (e.g., steep or shallow) lead to different areas of identical projected velocity (see above). Thus, a change in velocity field changes the shape of the emission profile and thus the entire shape of the P Cygni line! Unfortunately, the results from this procedure are highly ambiguous in the majority of cases (Why?). Another, sometimes better method to investigate the velocity stratification will be provided by the diagnostics of the H_α-profile (Sects. 7.2/8.2).

4.3   Theoretical P Cygni profiles: Response to ion density and shape of the velocity field

Fig. 14 shows some exemplary theoretical P Cygni profiles, to illustrate the last two points regarding the response to ion density and velocity field.

The second and third panel ($\beta = 0.7$, 1.0, where β controls the steepness of the velocity field, see Sect. 5.2) show profiles that were calculated for a velocity field which is predicted by *the theory of radiation driven winds* (Sect. 5). The first panel is based upon a steeper velocity field, i.e. higher velocities near the star, whilst the fourth one refers to a shallower velocity field, i.e., the wind reaches higher velocities far from the stellar surface. (In how far is the value $\beta = 0.5$ coupled to the radiation driven wind theory?)

NOTE: The shallower the velocity field, the higher the emission!

In addition, the ion density has been varied. Plotted are profiles for very large densities, such that the profiles become saturated (dotted and dashed-dotted profiles), for a moderate (dashed) and a low (solid line) ion density. The difference in densities between each line is a factor of 10.
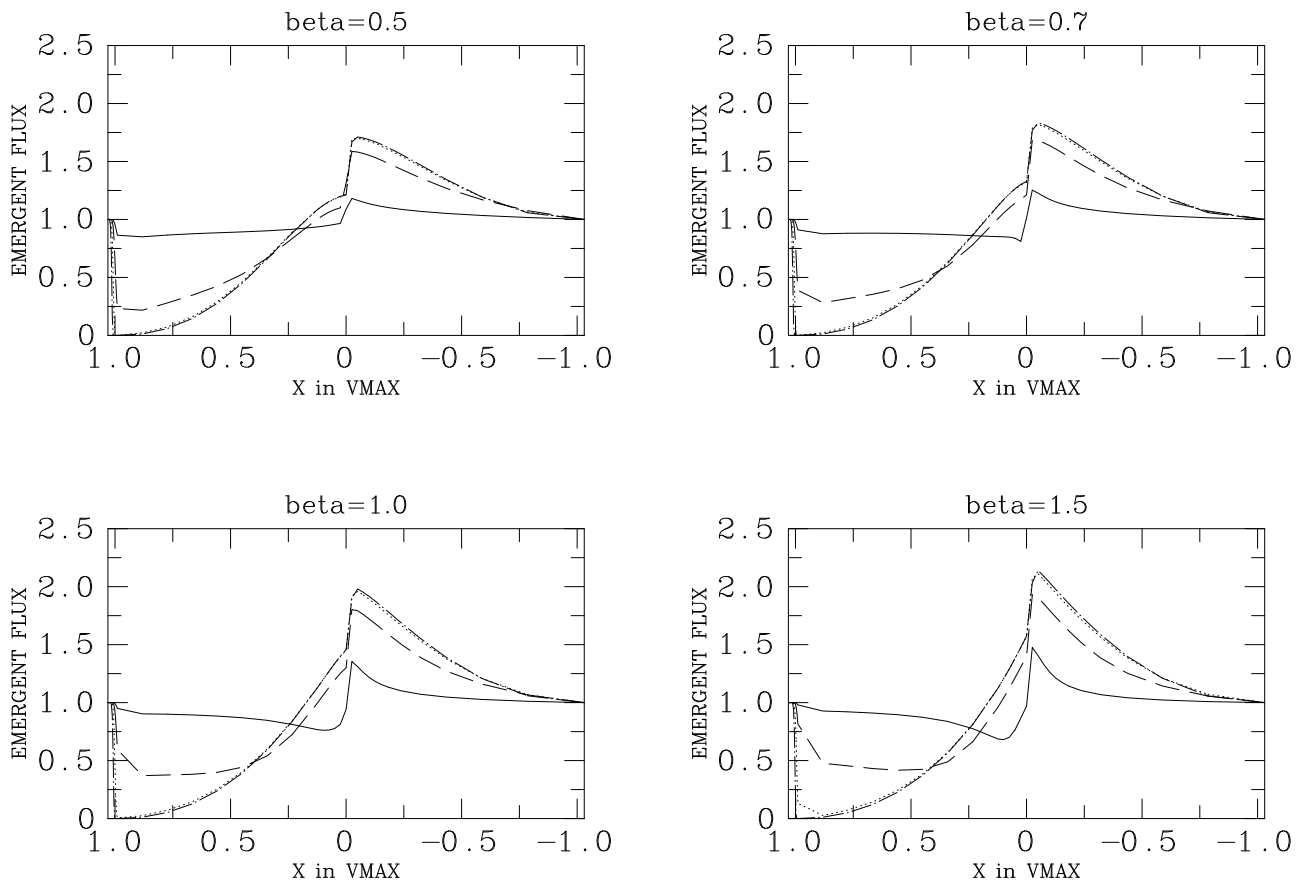
Figure 14: Response of theoretical P Cygni profiles to a variation of ion density (line strength) and velocity field. See text.

In all figures it was assumed that the ion density varies proportional to the total wind density. For different assumptions on this relation, completely different line shapes can arise, as you will see during your lab work.

NOTE: From a certain threshold on, the profiles are no longer changing when the ion density is further increased. This is the reason to call such profiles *saturated*!

Doublets: superposition of two profiles

A closer look at the *observed* P Cygni profiles (e.g., Sect. 3) reveals that all but the N IV $\lambda 1720$ line consist of two components. This is because most of the UV resonance lines from a certain ion have two different ground states[7] with very similar energies (both of which can be radiatively excited). This means, that these profiles consist of two superimposed P Cygni components, called *doublets*. This fact has to be accounted for in the simulation and analysis, of course.

Regarding the determination of v_∞, this quantity still can be read off the blue edge of the *composite profile*. One just has to translate the frequency shift *with respect to the transition*

---

[7]due to fine-structure splitting
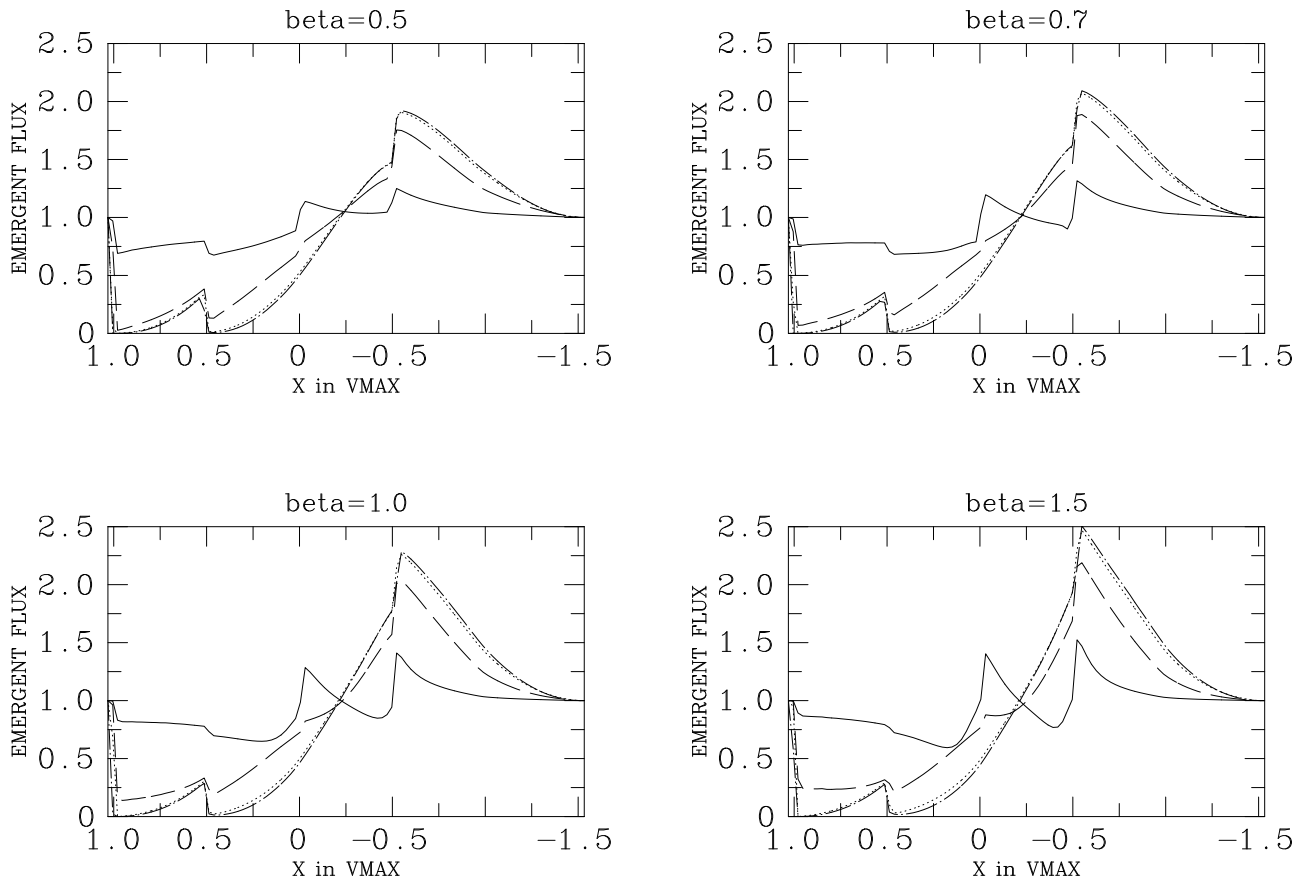
Figure 15: As Fig. 14, but for P Cygni *doublets.*

frequency of the blue component to velocity space. The dependence on velocity field and ion density is apparent from Fig. 15. In this figure, we assumed two components, separated corresponding to 0.5 v_∞. Obviously, the principal behavior compared to the singlet case (Fig. 14) does not change!

5   Theory of radiation driven winds – an introduction

In the following we'll have a somewhat closer look into the radiative line acceleration in hot star winds. In particular, we want to show how this acceleration mechanism leads to certain scaling relations for the winds' gross properties, $\dot{M}$ and v_∞. Moreover, we will illustrate that a smart combination of these relations in connection with atomic physics allows for the possibility of using hot stars as distance indicators, and provides a rather simple method for testing the theory itself.

Obviously, our simplified presentation can just explain some basic findings. As usual, real life is much more complex. For those of you who are interested in more details, we refer to the reviews (and literature cited therein) mentioned in Sect. 0.

5.1   The radiative line acceleration

In the following, we will assume the most simple model of a stellar wind, namely a model which is *spherically symmetric*, *stationary*, *homogeneous* and *free of magnetic fields*. All these assumptions need to be relaxed if certain more or less subtle observational facts are to be considered. Note, however, that the majority of observations indeed *can* be explained based on such a simple model, except for the assumption of homogeneity (see Sect. 10).

5.1.1   Momentum transfer via line absorption/emission

Let us begin by considering the momentum transfer due to the absorption and emission of stellar photons in a spectral line (with transition frequency ν_i in the atomic rest frame), where we will neglect the finite width[8] of the line profile[9]. During these processes, the absorbed ("in") and emitted ("out") photons transfer a net *radial* momentum

$$\Delta P_{\text{radial}} = \frac{h}{c} \left(\nu_{\text{in}} \cos \theta_{\text{in}} - \nu_{\text{out}} \cos \theta_{\text{out}} \right) \tag{1}$$

to the absorbing/emitting ion. θ is the angle between the direction of the photon and the radial unit vector (parallel to the velocity vector) of the ion.

Thanks to equal probabilities of emitting into the inward and the outward direction, respectively, the corresponding mean value are

$$\langle \cos \theta_{\text{out}} \rangle = 0 \tag{2}$$

and

$$\langle \cos \theta_{\text{in}} \rangle \approx 1, \tag{3}$$

since prior to the interaction the photons are approaching from the starward direction, i.e., they propagate in parallel to the velocity vector. Averaging yields

$$\langle \Delta P_{\text{radial}} \rangle = \frac{h \nu_{\text{in}}}{c}. \tag{4}$$

Let us now examine the situation sketched in Fig. 16 which displays the section of an arbitrary (spherical) shell of the wind, inside which the velocity increases by dv on a scale dr.

---

[8]because of thermal motions.

[9]This assumption is justified in hot star winds, since the thermal line width is small compared to Doppler shifts due to the velocity field.
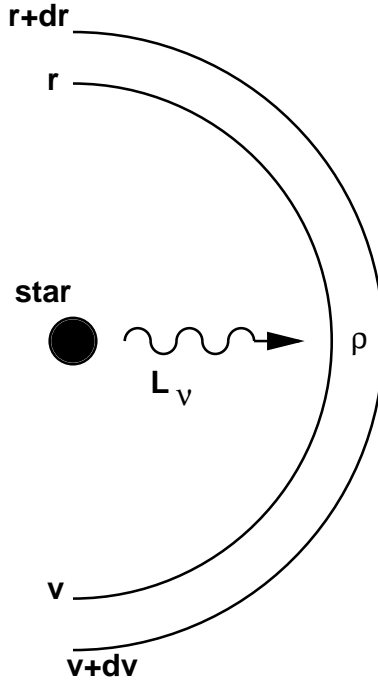
Figure 16: Sketch of a blue supergiant irradiating an arbitrary wind shell. L_ν is the spectral luminosity at frequency ν, v is the wind velocity at radius r and ρ the local density. The shell has a mass of $dm = 4\pi r^2 \rho dr$.

Photons emitted from the stellar surface (photosphere) with observer's frame frequency = start frequency ν_{obs} can be absorbed by an ion if their frequency in the *atomic* frame equals the transition frequency ν_{i}. Due to the Doppler effect and assuming that the photons propagate radially, i.e., that projected velocity = radial velocity, both frequencies are related via

$$
\begin{aligned}
\nu_{\mathrm{i}} &= \nu_{\mathrm{obs}} - \frac{\nu_{\mathrm{i}}}{c} v \\
\nu_{\mathrm{i}} &= (\nu_{\mathrm{obs}} + d\nu_{\mathrm{obs}}) - \frac{\nu_{\mathrm{i}}}{c}(v + dv).
\end{aligned}
\tag{5}
$$

In other words: a possible absorption/re-emission process (henceforth called "scattering" event) at higher velocities requires photons which have started at higher frequencies as well. (cf. Sect. 4.1). The frequency interval corresponding to the velocity interval dv is given via Eq. 5 as

$$
d\nu_{\mathrm{obs}} = \nu_{\mathrm{i}} \frac{dv}{c}.
\tag{6}
$$

The radiative acceleration of the shell "caused" by the considered line can be calculated using the general definition of any acceleration,

$$
g_{\mathrm{rad}}^{\mathrm{i}} = \frac{\Delta P}{\Delta t \Delta m}.
\tag{7}
$$

In our case, the line acceleration is obtained by multiplying the average momentum transferred due to a single scattering event with the number of available photons in the corresponding frequency interval, per time and per mass of the accelerated shell. The number of photons per time is

$$
\frac{N_\nu}{\Delta t} = \frac{\Delta(E_\nu/h\nu)}{\Delta t} = \frac{L_\nu \Delta\nu_{\mathrm{obs}}}{h\nu_{\mathrm{obs}}}
\tag{8}
$$

with L_ν the stellar luminosity (= radiated energy per time and frequency) at frequency ν. With $\nu_{\text{in}} = \nu_{\text{obs}}$, the (radial) acceleration of the shell caused by a single line results in

$$g_{\text{rad}}^{\text{i}} = \frac{N_\nu \langle \Delta P_{\text{radial}} \rangle}{\Delta t \Delta m} = \frac{L_\nu \Delta \nu_{\text{obs}}}{h \nu_{\text{obs}}} \frac{h \nu_{\text{obs}}}{c} \frac{1}{\Delta m} = \frac{L_\nu \nu_{\text{i}}}{c^2} \frac{\mathrm{d}v}{\mathrm{d}r} \frac{1}{4\pi r^2 \rho}. \tag{9}$$

Thus, the radiative line acceleration *of the shell* depends on the velocity gradient *inside the shell*! (whew, ponder, ponder, ???) A very strange and possibly unique dependency in physics!

Up to now we assumed tacitly that *all* photons (with matching frequency) which encounter the considered ionic species will be absorbed. Of course, this might not always be the case, and actually occurs only if *enough* absorbing ions are present. In other words: so far, we implicitly adopted a unit interaction probability. Consequently, the derived acceleration did not depend on any atomic property, but "only" on radiation field and the hydrodynamic structure. Allowing now for a *limited* interaction probability, this is given by

$$P_{\text{inter}} = 1 - \mathrm{e}^{-\tau} \tag{10}$$

where τ is the optical depth of the observed transition at $r, v, \mathrm{d}v$ etc. (see below).

By means of this probability, two distinct line types become apparent. For lines with $\tau \gg 1$ (i.e., numerous absorbing ions, so-called optically thick lines), we obtain $P_{\text{inter}} \approx 1$, whilst for optically thin lines with $\tau \ll 1$ we find $P_{\text{inter}} \approx \tau$. Thus, the radiative acceleration due to an optically thin line is a factor of τ smaller than due to an optically thick line.

Consequently, from here on we will use the (minor) approximation that all lines with $\tau \geq 1$ can be considered as optically thick and "behave" according to Eq. 9, whereas lines with $\tau < 1$ are defined as optically thin. The acceleration due to these lines needs to be modified by a factor corresponding to the local optical depth, depending on details of the considered transition. (Compare to the analogue difference between saturated and unsaturated P Cygni profiles, as described in Sect. 4).

5.1.2 Line ensemble

In fact, not just a single line but a (large) number of lines (several millions!) are present over the entire spectrum, which potentially can absorb radiation and momentum. From these zillions of lines, however, "only" some ten thousand are relevant for the overall line acceleration, $g_{\text{rad}}^{\text{tot}}$, because the rest has too low an interaction probability or lies in a spectral range where the photon density is very small.

In order to calculate the total line acceleration, we have to sum up all individual contributions and obtain (using the above approximation of dividing the lines into optically thick and thin ones)

$$\begin{aligned} g_{\text{rad}}^{\text{tot}} &= \sum_{\text{thin}} g_{\text{rad}}^{\text{i}} + \sum_{\text{thick}} g_{\text{rad}}^{\text{i}} \\ &= \frac{1}{4\pi r^2 c^2} \Big(\sum_{\text{thin}} L_\nu \nu_{\text{i}} \frac{\mathrm{d}v}{\mathrm{d}r} \frac{\tau_i}{\rho} + \sum_{\text{thick}} L_\nu \nu_{\text{i}} \frac{\mathrm{d}v}{\mathrm{d}r} \frac{1}{\rho} \Big). \end{aligned} \tag{11}$$

The optical depth of the lines can be expressed (within the so-called "Sobolev-" or supersonic approximation) as a function of velocity gradient, density and *line-strength*, k_i,

$$\tau_i = \frac{k_i \rho}{\mathrm{d}v/\mathrm{d}r}, \tag{12}$$
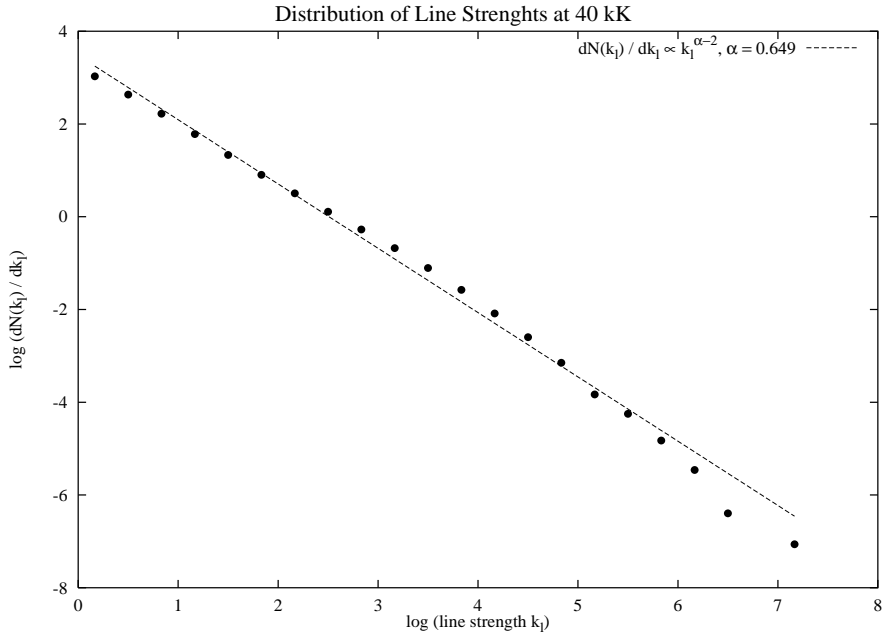
Figure 17: Line-strength distribution function (logarithmic) of a stellar wind model with $T_{\text{eff}} = 40,000$ K, as resulting from detailed model atmosphere calculations (dotted). Dashed line: corresponding power law fit according to Eq. 15.

where the line-strength comprises all atomic and plasma physical details of the affected transition (most importantly, occupation number of the absorbing level and cross-section), and remains basically constant throughout the wind.[10]

In fact, k_i should be dimensionless, and there are two additional normalization factors missing on the right-hand side of Eq. 12. (Which could that be? Hint: Remember that k_i contains the cross-section (per unit-mass) of the considered transition). For reasons of simplicity, however, we will proceed with the above definition.

Consequently, the limiting line-strength k_1, which separates optically thin from optically thick lines, depends only on the (local) wind properties,

$$1 = \frac{k_1 \rho}{\mathrm{d}v/\mathrm{d}r} \;\; \rightarrow \;\; k_1 = \frac{\mathrm{d}v/\mathrm{d}r}{\rho}. \tag{13}$$

Note that k_1 might vary across the wind, contrasted to k_i. By means of this quantity, it is possible to express the total radiative acceleration as

$$g_{\text{rad}}^{\text{tot}} = \frac{1}{4\pi r^2 c^2}\Big(\sum_{k_i < k_1} L_\nu \nu_i k_i \; + \; k_1 \sum_{k_i \geq k_1} L_\nu \nu_i \Big), \tag{14}$$

which immediately shows the "saturation effect" from another perspective: all optically thick lines behave the same, whilst optically thin lines react according to their line-strengths.

To exploit this relation, we still need the number and line-strengths of the optically thin lines, and the number of the optically thick ones, or, in other words, the line-strength distribution. Interestingly, it turns out that this distribution can be expressed in rather simple terms (see

---

[10]at least for the majority of the driving lines.

Fig. 17): The number of lines in a frequency interval $\nu, \nu + \mathrm{d}\nu$ with line-strengths $k_i, k_i + \mathrm{d}k_i$ can be approximated by a power law,

$$\mathrm{d}N(\nu, k_i) = - N_\mathrm{o}\, f_\nu(\nu)\, k_i^{\alpha-2}\, \mathrm{d}\nu\, \mathrm{d}k_i, \ 0 < \alpha < 1, \tag{15}$$

where the frequency distribution is *independent* of the line-strength distribution! (the dimensions suppressed so far accumulate in the definition of N_o.) Replacing the sums in Eq. 14 by corresponding (double-)integrals and using (15), one finds

$$
\begin{aligned}
g_\mathrm{rad}^\mathrm{tot} &= \frac{1}{4\pi r^2 c^2} \left\{ \int_0^\infty \int_0^{k_1} k_i L_\nu \nu\, \mathrm{d}N \ + \ k_1 \int_0^\infty \int_{k_1}^\infty L_\nu \nu\, \mathrm{d}N \right\} \\
&= \frac{N_\mathrm{o} \int_0^\infty L_\nu \nu f_\nu(\nu)\, \mathrm{d}\nu}{4\pi r^2 c^2} \left\{ \frac{1}{\alpha} k_1^\alpha + \frac{1}{1-\alpha} k_1^\alpha \right\}
\end{aligned}
\tag{16}
$$

The second equation illustrates two points. (i) Both the acceleration from optically thick and thin lines scale with the same power α of k_1. (ii) The ratio of these accelerations is given by $\alpha/(1-\alpha)$, and corresponds to a factor of 2 at a value of $\alpha \approx 2/3$ (see Fig. 17).

Our FINAL RESULT for the total line acceleration can be summarized as

$$g_\mathrm{rad}^\mathrm{tot} = \frac{\mathrm{const}}{4\pi r^2} \Big(\frac{\mathrm{d}v/\mathrm{d}r}{\rho} \Big)^\alpha, \tag{17}$$

and depends, except for the scaling factor and the exponent, only on hydrodynamical quantities. (The real challenge of wind calculations, however, is to calculate just these two quantities, which depend on the occupation numbers of all contributing levels.)

5.2 Solution of the equation of motion

After we have found a (relatively simple) expression for the line acceleration, we can now begin to study the hydrodynamical structure of the wind. To this end, we have to consider the hydrodynamical equations (for stationary, spherically symmetric flows):

1. the equation of continuity: $\dot{M} = 4\pi r^2 \rho v$,

2. the equation of momentum: $v\frac{\mathrm{d}v}{\mathrm{d}r} = -\frac{1}{\rho}\frac{\mathrm{d}p}{\mathrm{d}r} - g_\mathrm{grav}(1-\Gamma) + g_\mathrm{rad}^\mathrm{tot}$,

3. the equation of state: $p = \rho a^2$,

where p is the pressure, a the isothermal sound velocity, g_grav the gravitational acceleration of the star and Γ the ratio between Thomson acceleration (radiative acceleration due to photon scattering at free electrons, $\propto r^{-2}$) and gravitational acceleration. Note: $\Gamma < 1$ for stable stars, $\Gamma = \mathrm{O}(0.5)$ for supergiants.

Let us now solve these equations for the major, supersonic part $(v > a)$ of the wind. In this range, the pressure forces can be neglected, and by inserting the equation of continuity and using Eq. 17, the equation of motion of the wind reads

$$r^2 v \frac{\mathrm{d}v}{\mathrm{d}r} = -GM(1-\Gamma) \ + \ C' L \dot{M}^{-\alpha} \big(r^2 v \frac{\mathrm{d}v}{\mathrm{d}r}\big)^\alpha, \tag{18}$$

with M the stellar mass, stellar luminosity $L = \int L_\nu \mathrm{d}\nu$ and constant C'. (Express C' in terms of previously defined quantities.)

The equation of motion can be readily solved (e.g. graphically), by using the variable $z = r^2 v \mathrm{d}v/\mathrm{d}r$, where z needs to be constant throughout the wind to allow for a *unique* solution (since all other quantities are constant as well). In order to obtain such a unique solution, the mass-loss rate is constrained by

$$\dot{M} \propto L^{\frac{1}{\alpha}} \left(M(1 - \Gamma) \right)^{1 - \frac{1}{\alpha}}, \tag{19}$$

whilst from $z =$const the velocity law is obtained via a simple integration, *independent from the mass-loss rate*,

$$
\begin{aligned}
v(r) &= v_\infty \left(1 - \frac{R_*}{r} \right)^{\frac{1}{2}} \\
v_\infty &= \left(\frac{\alpha}{1 - \alpha} \right)^{\frac{1}{2}} \left(\frac{2GM(1 - \Gamma)}{R_*} \right)^{\frac{1}{2}}.
\end{aligned}
\tag{20}
$$

R_* is the stellar radius and the second factor (which majorly determines v_∞) is the (photospheric) escape velocity, v_{esc}. (From this expression, explain the difference of the "observed" terminal velocities of A-supergiants and O-dwarfs, cf. Sect. 1.2.2).

Due to the various approximations used so far, the above derivation of the wind properties is highly simplified. When carrying out a more detailed analysis discarding all simplifications, however, no dramatic changes will occur. Most importantly, the scaling relation for $\dot{M}$ remains unaltered, and also the proportionality $v_\infty \propto v_{\mathrm{esc}}$ does not change, though the constant of proportionality becomes different. The most severe change affects the *shape* of the velocity field. Here, the exponent 1/2 needs to be modified,

$$v(r) = v_\infty \left(1 - \frac{R_*}{r} \right)^{\beta}, \tag{21}$$

with $\beta \approx 0.8$ in most cases. This exponent β corresponds to the quantity introduced in Sect. 4.3.

5.3 The Wind-momentum Luminosity Relation (WLR)

One of the most important consequences of the above scaling relations concerns the theoretical explanation of the so-called Wind-momentum Luminosity Relation (WLR), which has been discovered by Kudritzki et al. [11] on a purely empirical basis.

With respect to Galactic supergiants, the "observed" WLR (the one you should derive during this lab) can be written as follows,

$$\dot{M} v_\infty (R_*/R_\odot)^{\frac{1}{2}} \propto L^{1.46}, \tag{22}$$

i.e., the wind-momentum rate, modified by the square of the stellar radius, depends on some power of the stellar luminosity alone. By means of our theoretical scaling relations, on the other hand, we find

$$\dot{M} v_\infty (R_*/R_\odot)^{\frac{1}{2}} \propto L^{\frac{1}{\alpha}} \left(M(1 - \Gamma) \right)^{\frac{3}{2} - \frac{1}{\alpha}}, \tag{23}$$

which, at first glance, displays a significant difference in terms of an additional mass dependence. But, if we remember that $\alpha \approx 2/3$ (Fig. 17), this dependence vanishes almost completely. Consistently, the exponent from the empirical relation corresponds to an α-value of 0.68!

---

[11] Kudritzki, R.P., Lennon, D.J., Puls, J., 1995, "Quantitative Spectroscopy of Luminous Blue Stars in Distant Galaxies". In: ESO Astrophysics Symposia, Science with the VLT, eds. J.R. Walsh and I.J. Danziger, Springer, Heidelberg, p. 246

Summarizing, the observed WLR can be explained as a consequence of the scaling relations for line-driven winds, *plus* an exponent of the line-strength distribution function being close to $\alpha = 2/3$. Since the latter condition is strongly related to atomic physics, and the WLR might be used to measure extra-galactic distances (see below), in the end a micro-physical result allows for the measurement of literally astronomical quantities.

Distance measurements.   The corresponding strategy is as follows. In the recent years and still now, various working groups dealing with hot stars (including the "hot-star" group from our institute) develop(ed) corresponding *empirical* relations for objects with *known* distances, in dependence of the atmospheric "metallicity", i.e., chemical composition. (Why is there such a dependence?). This is done in the same way as you will do it for Galactic O-supergiants during this lab. Once such relations are available, the distance to a specific star can be determined in the following way:

- the effective temperature, T_{eff}, of the star can be derived from the analysis of photospheric lines, as well as its metallicity.

- The terminal velocity is measured from P Cygni profiles.

- The quantity $Q = \dot{M}/(R_*/R_\odot)^{3/2}$ is determined from H_α-lines (see chap. 7.2). (Note that this is the actual measurement quantity).

For the derived metallicity, one then uses the appropriate WLR, always of the form

$$\log(\dot{M}v_\infty(R_*/R_\odot)^{\frac{1}{2}}) = x\log(L/L_\odot) + b \tag{24}$$

where x is its logarithmic slope[12], and b is the offset of the relation, primarily dependent on the metallicity of the wind. Inverting the above equation, the stellar radius can be calculated via

$$\log(R_*/R_\odot) = \frac{\log Q + \log v_\infty - 4x\log(T_{\mathrm{eff}}/T_{\mathrm{eff}\odot}) - b}{2x - 2}. \tag{25}$$

The distance to the star then follow from the radius, the observed stellar brightness and the reddening (cf. Sect. 9.2). Typical errors for the distance modulus of the host galaxy are within $\pm 0.1^{\mathrm{m}}$, if some 20 objects with winds have been analyzed in the above manner.

Such errors compare well with those from more common methods to determine distances on intermediate scales (e.g., exploiting the period-luminosity-relation of Cepheids), and enable an *independent* check. First such measurements gave very promising results.

Testing the theory.   Besides being applied for distances measurements, the WLR is meanwhile the most frequently used tool for testing the theory itself. One "simply" has to compare the observed with the corresponding theoretical WLR, and can check for potential errors. (For this application, the stellar distances ($\to R_*$) have to be known, of course). The advantage of using the WLR instead of the individual quantities ($\dot{M}, v_\infty$) lies in the fact that the WLR is almost independent of stellar mass and Eddington-Γ, noting that these parameters are usually difficult to measure. Moreover, the product of $\dot{M}$ and v_∞ is a much more stable number in numerical simulations than the individual quantities.

From such comparisons, a variety of problems could be identified in recent years. Most importantly, the problem of wind-clumping (inhomogeneities) and the so-called weak wind problem emerged, see Sect. 10.

---

[12]related to the slope of the line-strength distribution function.

6   Analysis of UV P Cygni profiles – determination of physical parameters

From the fits to the observed line profiles (performed during the first afternoon of the lab), one cannot only obtain values for v_∞, but also quantities which are related to the stratification of the line opacities and thus of the occupation numbers.

Particularly if the profiles are *not* saturated, one can derive a variety of interesting quantities and compare with theoretical predictions. We will denote the corresponding variables by k and α (as in the fit-programme, not to be confused with the similarly named quantities from Sect. 5), and show in how far these quantities can be translated to more physical wind parameters.

Specifically, if one parameterizes the occupation number density, $n_{ljk}(v)$, of the lower, absorbing level in terms of mass density and chemical abundance, one can derive information regarding the product of mass-loss rate, $\dot{M}$, and ionization fraction, $X(v)$, from the line profile.

The optical depth introduced in Eq. 12 can be alternatively written as follows, *if from here on we measure velocities in units of v_∞ and radii in units of R_*,*

$$\tau(v) = \bar{\chi}_{\mathrm{i}}(v)\,\lambda_{lu}\,\frac{R_*}{v_\infty}\,\frac{1}{\mathrm{d}v/\mathrm{d}r} \ := \ \frac{\overline{\kappa}(v)}{\mathrm{d}v/\mathrm{d}r} \tag{26}$$

$$\text{with}\qquad \overline{\kappa}(v) \ := \ \frac{\pi e^2}{m_{\mathrm{e}}c}\,\frac{\lambda_{lu}R_*}{v_\infty}\,f_{lu}\,n_{ljk}(v). \tag{27}$$

$\bar{\chi}_{\mathrm{i}}$ is the frequency integrated line opacity, and λ_{lu} the wavelength of the considered transition. In the definition of $\overline{\kappa}$ (Eq. 27), which corresponds to an adequately scaled opacity, the first factor is the classical absorption cross section, whilst f_{lu} is the quantum-mechanic correction, the so-called oscillator strength. Moreover, we have neglected any (negative) contribution from induced emission, which is low in the UV.

The occupation number density n_{ljk} of level l in ionization stage j of element k can be expressed in terms of excitation fraction E, ionization fraction X and relative abundance of the element (with respect to hydrogen), A_{k},

$$n_{ljk} = \frac{n_{ljk}}{n_{jk}}\,\frac{n_{jk}}{n_k}\,\frac{n_k}{n_{\mathrm{H}}}\,n_{\mathrm{H}} \tag{28}$$

$$\frac{n_{ljk}}{n_{jk}} = E(v), \quad \frac{n_{jk}}{n_k} = X(v), \quad \frac{n_k}{n_{\mathrm{H}}} = A_{\mathrm{k}}.$$

A_{k} is assumed to be constant within the entire atmosphere. With respect to the conversion between mass and particle densities we assume that the bulk of the (wind) material consists of hydrogen and helium, which is well justified for OB-stars which are not too far developed,

$$n_{\mathrm{H}}(v) = \frac{\rho(v)}{m_{\mathrm{H}}(1 + 4Y_{\mathrm{He}})}\,, \quad Y_{\mathrm{He}} = n_{\mathrm{He}}/n_{\mathrm{H}}. \tag{29}$$

Y_{He} is the relative abundance of helium with respect to hydrogen, and m_{H} is the mass of the hydrogen atom. The mass density $\rho(v)$ results from the equation of continuity, see Sect. 5.2,

$$\rho(v) = \frac{\dot{M}}{4\pi\,R_*^2 v_\infty\,r^2 v}.$$

Combining with the previous two equations, we obtain

$$n_{ljk}(v) = E(v)X(v)\,\frac{A_{\mathrm{k}}\,\dot{M}}{4\pi\,R_*^2 v_\infty\,m_{\mathrm{H}}(1 + 4Y_{\mathrm{He}})}\,\frac{1}{r^2 v}. \tag{30}$$

Comparison of Eq. 27 with Eq. 30 shows that the scaled opacity, $\overline{\kappa}(v)$, varies with $1/(r^2v)$, i.e., *is proportional to the mass density*, as long as the ionization fraction remains constant. Thus, we introduce the parameter $k(v)$ (mentioned already above) as a fit parameter, which is proportional to the line-strength k_i (cf. Eq. 12):

$$\overline{\kappa}(v) := k(v)\,\frac{1}{r^2v} \;\Rightarrow\; \tau(v) = \frac{k(v)}{r^2v\mathrm{d}v/\mathrm{d}r} \tag{31}$$

i.e.,

$$k(v) = E(v)X(v)\,\frac{\dot{M}}{R_*v_\infty^2}\,\frac{(\pi e^2)/(m_\mathrm{e}c)}{4\pi m_\mathrm{H}}\,\frac{A_\mathrm{k}}{1+4Y_\mathrm{He}}\,f_{lu}\lambda_{lu}. \tag{32}$$

Except for $E(v)$ and $X(v)$, there are only constants left, i.e., $k(v)$ directly parameterizes the ratio between occupation number density $n_{ljk}(v)$ and mass density $\rho(v)$. In the following, we set $E(v) = 1$, since during this lab we are dealing with *resonance lines* only, which originate from the ground state. Thus, the corresponding occupation numbers are fairly equal to the total population of the considered ionization stage, $n_{lkj}(v) \approx n_{jk}(v)$. In this case, $k(v)$ *is directly proportional to the ionization fraction $X(v)$*:

$$\dot{M}X(v) \;=\; \frac{4\pi m_\mathrm{H}\,(\,1+4Y_\mathrm{He}\,)}{\frac{\pi e^2}{m_\mathrm{e}c}\,f_{lu}\lambda_{lu}\,A_\mathrm{k}}\,R_*v_\infty^2\,k(v) \tag{33}$$

By measuring $k(v)$, we can immediately derive the *product* of mass-loss rate and ionization fraction. However, we also meet one of the central problems inherent to the analysis of UV P Cygni profiles: The determination of the mass-loss rate from resonance lines alone can be extremely biased, due to the rather uncertain knowledge of the ionization fraction, $X(v)$.

All other quantities $(R_*, v_\infty, A_\mathrm{k}, Y_\mathrm{He})$ are usually known with sufficient precision. The stratification of the the ionization fraction, $X(v)$, on the other hand, cannot be derived by means of a purely empirical diagnostic method based on UV spectra alone. Either, a numerical atmospheric model is required which predicts all occupation numbers with sufficient precision (then, $\dot{M}$ can be derived via Eq. 33 and the theoretical values for $X(v)$), or the mass-loss rate needs to be known from other diagnostics, e.g., from the optical H_α-line, see Sect. 7. In the latter case then, one can derive $X(v)$ and compare with theoretical predictions.

A frequently used quantity, which can be directly derived from the line fits, is the *column density* N^col of the absorbers (in cm^{-2}) between two positions in the wind,

$$\begin{aligned}
N^\mathrm{col}(v_1, v_2) &= \int_{R_1}^{R_2} n_{ljk}(R)\,\mathrm{d}R \;=\; R_* \int_{v_1}^{v_2} n_{ljk}(v)\Big(\frac{\mathrm{d}v}{\mathrm{d}r}\Big)^{-1}\mathrm{d}v = \\[4pt]
&\quad \left[n_{ljk}(v) = \frac{m_\mathrm{e}c}{\pi e^2}\,\frac{1}{f_{lu}\lambda_{lu}}\,\frac{v_\infty}{R_*}\,\frac{k(v)}{r^2v}\right] \\[4pt]
&= \frac{m_\mathrm{e}c}{\pi e^2}\,\frac{v_\infty}{f_{lu}\lambda_{lu}}\int_{v_1}^{v_2}\frac{k(v)}{r^2v\mathrm{d}v/\mathrm{d}r}\,\mathrm{d}v \;=\; \frac{m_\mathrm{e}c}{\pi e^2}\,\frac{v_\infty}{f_{lu}\lambda_{lu}}\int_{v_1}^{v_2}\tau(v)\,\mathrm{d}v.
\end{aligned} \tag{34}$$

From here on, we will use the generalized β-velocity law (Eq. 21) to describe the velocity field, with a certain modification compared to the original definition,

$$v(r) = \Big(1 - \frac{b}{r}\Big)^\beta, b = 1 - v_\mathrm{min}^{1/\beta}. \tag{35}$$

Remember that all radii and velocities, e.g., r, v and $v_{\min}$, have been expressed in normalized units. By introducing the parameter b, we allow that the wind already starts with a certain initial speed (which should be of the order of the speed of sound, $v_{\min} \approx 0.01$ in units of v_∞). In this way we account for the fact that below the sonic point the pressure terms begin to dominate (see Sect. 5.2), such that the β-field becomes invalid there. (What is the corresponding law of the velocity field below the sonic point?)

Moreover, we approximate the stratification of the ionization by a power-law with respect to velocity (this is the most simple possibility, there are other and more appropriate methods), i.e.,

$$k(v) = k_o v^\alpha \tag{36}$$

(same notation in the the fit-programme). Because of $\max(v) = 1$, k_o corresponds to the degree of ionization in the outermost wind part, whereas $\alpha > 0 (< 0)$ corresponds to a degree of ionization which decreases (increases) towards the star. $\alpha = 0$ corresponds to constant ionization, of course.

With these definitions (Eqs. 35, 36) and the quantities β, k_o and α derived from your line fits, the column density (Eq. 34) can be estimated,

$$N^{\mathrm{col}}(v_1, v_2) = \frac{m_e c}{\pi e^2} \frac{v_\infty}{f_{lu}\lambda_{lu}} \frac{k_o}{\beta b} \int_{v_1}^{v_2} v^{1/\beta - 2 + \alpha}\, \mathrm{d}v \tag{37}$$

(derive Eq. 37). This quantity does not provide information regarding the *run* of the ionization, of course. Let us finally define a "mean ionization fraction", $\overline{X}$, as the ratio between the occupation number of a certain ion and the total particle number of the corresponding element, both evaluated over the column as introduced above,

$$
\begin{aligned}
\overline{X}_k &= \frac{\int_{r_1}^{r_2} n_{jk}(r)\,\mathrm{d}r}{\int_{r_1}^{r_2} n_k(r)\,\mathrm{d}r} = \frac{\int_{r_1}^{r_2} X_k(r) n_{\mathrm{H}}(r)\,\mathrm{d}r}{\int_{r_1}^{r_2} n_{\mathrm{H}}(r)\,\mathrm{d}r} = \frac{\int_{r_1}^{r_2} X_k(v)/(r^2 v)\,\mathrm{d}r}{\int_{r_1}^{r_2} 1/(r^2 v)\,\mathrm{d}r} = \\[2mm]
&= \frac{4\pi m_{\mathrm{H}}\left(1 + 4Y_{\mathrm{He}}\right)}{\dot{M}\frac{\pi e^2}{m_e c} f_{lu}\lambda_{lu} A_{\mathrm{k}}} R_* v_\infty^2 \left\{ \frac{\int_{v_1}^{v_2} k(v)\mathrm{d}v / (r^2 v \mathrm{d}v/\mathrm{d}r)}{\int_{v_1}^{v_2} \mathrm{d}v / (r^2 v \mathrm{d}v/\mathrm{d}r)} \right\} = \\[2mm]
&= \frac{4\pi m_{\mathrm{H}}\left(1 + 4Y_{\mathrm{He}}\right)}{\dot{M} A_k} \beta b\, R_* v_\infty\, N^{\mathrm{col}}(v_1, v_2) \left(\int_{v_1}^{v_2} v^{1/\beta - 2}\,\mathrm{d}v \right)^{-1}.
\end{aligned}
\tag{38}
$$

Note that also the calculation of the mean ionization fraction requires the knowledge of $\dot{M}$!

7   Analysis of the H_α-profile

In this last "theoretical section", we will clarify how the mass-loss rates from stellar winds can be measured. During recent years, it turned out that the H_α line[13] is a particularly well suited indicator.

---

[13]transition between level 2 and 3 of the hydrogen atom.

7.1   Why H_α?

The reason is the coincidence of three favorable conditions:

1. The H_α line is a so-called ρ^2 *line*.
   In contrast to resonance lines (particularly, the UV P Cygni lines discussed in the previous sections) with opacities proportional to the mass density (times a moderately varying factor indicating the change of ionization fraction), there are a multitude of lines (including H_α) due to transitions *between excited levels*, which under wind conditions are populated according to

   $$n_{l,j}(l \neq 1) \sim n_{\mathrm{e}} n_{j+1} f(T_{\mathrm{e}}, \ldots) \tag{39}$$

   ($n_{l,j}$: occupation number density of level l from ion j, T_{e}: electron temperature, n_{e}: electron density), i.e., their population is proportional to the product of the population of the next higher ion and the electron density.

   Consequently, the ratio between emission- and absorption coefficient, the so-called line source function, S^{L} (which basically depends on the ratio between the occupation numbers of the transition's upper and lower level), remains relatively constant throughout the wind, as long as this is warranted for the electron temperature, $T_{\mathrm{e}}(r)$. To a good approximation then, the line source function is fairly similar to the Planck function, $B_\nu(T_{\mathrm{e}})$.

   This behaviour follows from the fact that the dominating population mechanism for the excited levels is due to radiative recombinations from the next higher ion (electron + ion(j+1) $\rightarrow$ excited ion(j) + photon), followed by de-excitation cascades to lower levels, where the first process is a *thermal one*, because of the Maxwellian velocity distribution of the contributing particles (electrons and ions).

   For resonance lines, on the other hand, the line source function follows $S^{\mathrm{L}}_{\mathrm{resonance}} \sim 1/r^{2\ldots3}$, because resonance lines are due to (quasi-) *scattering* processes, i.e., the photon number remains conserved, whereas the number density becomes diluted with increasing wind volume.

   As we will see below, it is just this (almost) constant line source function which gives rise to the significantly different profile shape [14] of H_α, compared to P Cygni profiles (see also the title page of this manual).

   If the ionization stage $(j + 1)$ is the major one with a population $\propto \rho$ – as it is the case for H II in hot stars –, and also the electron density follows the mass-density,

   $$n_{l,j}(l \neq 1) \propto \rho^2, \tag{40}$$

   and the corresponding opacity has a similar dependence, $\bar{\chi}_{\mathrm{i}} \sim \rho^2$.

   In stellar winds, such so-called *recombination lines* are mostly in emission, and their strength ("equivalent width") increases with the *square* of the wind density (more precisely, with $\frac{\dot{M}^2}{R_\star^3 v_\infty^3}$, cf. Eq. 41); thus, they are better $\dot{M}$-indicators than resonance lines, at least as long as the wind densities are not too low. In the latter case, the wind emission is "hidden" inside the rather broad photospheric absorption component.

---

[14]Actually, such a strong difference is present "only" in OB stars, whilst the cooler A-supergiants display an H_α profile of P Cygni type: due to the different conditions, the ionization/excitation equilibrium of hydrogen changes, and the 2nd level becomes the *effective* ground-state, transforming H_α into a (quasi-) resonance line.

2. H_α is one of the strongest lines.
   Since we are looking for a sensible indicator of wind density, the diagnostic line needs to be strong (large oscillator strength, with significantly populated participating levels). The strongest ρ^2-line in the optical spectrum of O-stars is typically the HeII $\lambda4686$ line (with a rather complex formation mechanism), followed by H_α.

3. The behaviour of H_α is well understood.
   Contrasted to the HeII-lines, the behaviour of the hydrogen Balmer lines in O-stars is determined by well understood processes, and can be simulated in an almost perfect way, when compared with observations. The overall structure of the population is very *stable*, and rather insensitive to variations of stellar parameters (again contrasted to the HeII-lines, which react sensitively to somewhat marginal effects).

7.2 H_α-profile and mass-loss rate

In the following we will derive the relation between H_α-profile and mass-loss rate. To this end, we will use the same (Sobolev-) approximation as applied in previous sections to calculate the line optical depth. Again we also neglect the low metal content when estimating the product $n_e n_{HII}$ (see above; but remember that it is the metal lines which accelerate the wind), and consider only the elements H and He. Since both elements are almost completely ionized in O-stars,

$$n_e n_{HII} = \frac{1 + Y_{He} I_{He}}{(1 + 4 Y_{He})^2} \frac{\rho^2}{m_H^2} \tag{41}$$

(I_{He} : number of free electrons per helium atom = 2 in O-stars). In analogy to Eqs. 12 and 26, the optical depth is given by

$$\tau = \bar{\chi}_{H23}(r) \, \lambda_{H23} \frac{R_*}{v_\infty} \frac{1}{dv/dr} = \frac{A(r)}{r^4 v^2 dv/dr} \tag{42}$$

The function $A(r)$ comprises all parameters of the line transition, as well as the wind parameters. The (decisive) difference to the optical depth in resonance lines is the denominator: it contains *an additional* term $r^2 v$, because of the ρ^2 dependence of $\bar{\chi}_i$.

By expressing the excitation/ionization equilibrium in terms of the Saha-Boltzmann equation, and using the equation of continuity together with Eqs. (41, 42) and the the quantum-mechanical parameters of the transition, the quantity $A(r)$ reads

$$A(r) = \mathcal{F}_\alpha \cdot T_e^{-1.5} \left[b_2(r) \exp\left(\frac{3.945}{T_e} \right) - b_3(r) \exp\left(\frac{1.753}{T_e} \right) \right] \frac{1 + I_{He} Y}{(1 + 4Y)^2} \frac{\dot{M}^2}{R_*^3 v_\infty^3} \tag{43}$$

$$\text{with} \quad \mathcal{F}_\alpha = 49.3$$

($\dot{M}$ in $10^{-6} M_\odot/yr$, v_∞ in 1000 km/s, $R_\star$ in solar radii and T_e in 10^4 K). The leading factor $\mathcal{F}$ comprises all constants, conversion factors as well as wavelength and oscillator strength of the transition.

The small[15] deviations of the occupation numbers from their thermodynamic equilibrium value (Saha-Boltzmann) are considered in the form of the so-called *departure coefficients*,

$$b_i = \frac{n_i}{n_i^*}. \tag{44}$$

---

[15]only for the excited levels of hydrogen in O-star stellar winds; other levels (including the hydrogen ground state) are far away from the thermodynamic equilibrium.

They describe, for the present value of $n_e n_{j+1}$, the actual NLTE[16]-occupation numbers, n_i, in units of the thermodynamic equilibrium population, n_i^*. They are provided from numerical model calculations and used in our fit-programme. Since these deviations are small for the hydrogen levels 2 and 3 (see above), the departure coefficients are not too different from unity (this is one of the reasons to use H_α; for the involved levels of, e.g., He II $\lambda 4686$, the departure coefficients are much more complex).

Eq. 43 illustrates the principal difference between the scaling relations for resonance and recombination lines. While the optical depth of resonance lines depends on the combination $\dot{M}/(R_* v_\infty^2)$ (cf. Eq. 32), this becomes a function of $\dot{M}^2/(R_*^3 v_\infty^3)$ for recombination lines, because of the additional ρ- dependence.

   If the terminal speed is known and not altered during the fitting process, the shape of synthetic H_α-profiles should remain constant as long as the quantity $Q = \dot{M}/R_*^{3/2}$ remains constant. This is the reason why we have quoted this particular combination as the actual measuring quantity in Sect. 5.3.

   For typical OB-stars, the "wind parameter" A ranges from 10^{-7} to 10^{-1}, i.e., the H_α-line is optically thin in the largest part of the wind (cf. Eq. 42). In this region, the continuum is optically thin as well. Thus, for an approximate calculation of the profile we can neglect the contribution of the continuum, and only the line source function, $S^L(r)$, has to be considered. In Sobolev theory then, we find for the H_α-profile (in units of the continuum)

$$R_x(x > 0) = \frac{\frac{1}{2} \int_0^1 P_x e^{-\tau_s}\, p \mathrm{d}p + \frac{1}{2} \int_0^\infty \frac{S^L}{I_c} \left(1 - e^{-\tau_s}\right) p \mathrm{d}p}{\frac{1}{2} \int_0^1 p \mathrm{d}p}, \tag{45}$$

$$R_x(x < 0) = \frac{\frac{1}{2} \int_0^1 P_x\, p \mathrm{d}p + \frac{1}{2} \int_1^\infty \frac{S^L}{I_c} \left(1 - e^{-\tau_s}\right) p \mathrm{d}p}{\frac{1}{2} \int_0^1 p \mathrm{d}p}, \tag{46}$$

where $x = (\nu/\nu_0 - 1)c/v_\infty$ measures the frequency in units of velocity shift with respect to line center ($x > 0$: "blue" side of the line), P_x is the photospheric profile, and $I_c = B_\nu(T_{rad})$ is the continuum intensity at $x = 0$, i.e., at line center. The continuum I_c is calculated in terms of the Planck function B_ν, with T_{rad} the corresponding photospheric *radiation* temperature. The impact parameter, p, which is the integration variable, is defined in Fig. 18.

The interpretation of these relations (in connection with Fig. 18) is analogue to the formation of P Cygni profiles. The decisive difference is the stronger decrease of $\tau(v)$ towards outer regions, together with a line source function which remains basically constant (see Sect. 7.1).

   Again, the blue part of the profile, $R_x(x > 0)$, is formed by material that approaches the observer and by photons which are irradiated by the stellar core: The first integral refers to material in front of the disk which attenuates the *photospheric* H_α-profile, P_x. The wind emission is due to the 2nd integral, where the individual contributions are related to the sizes of the emitting areas: it has its maximum value at $x = 0$, and its minimum where τ vanishes. The maximum extent of the profile corresponds to $v = v_\infty$ ($x = 1$), if the absorber/emitter densities are still large enough far away from the star (this only happens for *very* dense winds).

   On the red side of the profile, $R_x(x < 0)$, one (i) observes the *unattenuated* photospheric profile, since at these frequencies the matter in front of the stellar disk cannot absorb. (ii) The emission is due to material from the backward hemisphere, (almost) symmetrical to the blue emission (except for the occulted region).

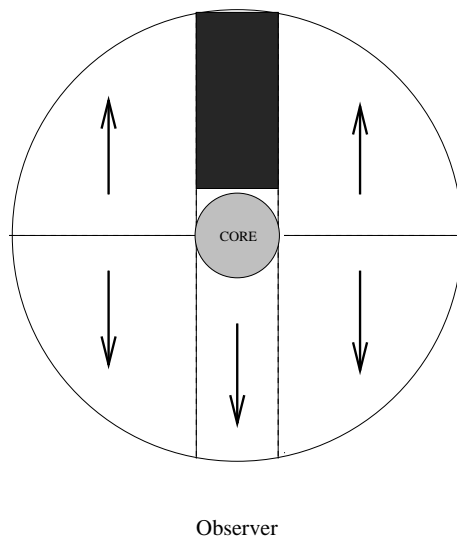[16] *non local thermodynamic equilibrium*

Observer

Figure 18: H$_\alpha$-line formation: sketch of different wind regions. In the left and right hand wind lobes, the observer sees approaching and departing matter. The dark region is not visible to the observer, and is responsible for the (slight) asymmetry of the observed profile (at least if there is no perfect local thermodynamic equilibrium). The so-called impact-parameter, p, varies along the horizontal axis. At the stellar center is has a value of "0", at the edge of the stellar core a value of "1", and increases towards larger values when moving away from the core.

In this way, the variation of H$_\alpha$ with increasing $\dot{M}$ can be easily understood. At low $\dot{M}$ and thus low τ, the first integrals dominate the profile on both sides. The factor $\exp(-\tau)$ is close to unity, and we see a symmetric photospheric line. With increasing $\dot{M}$, the 2nd integrals begin to contribute, and the photospheric profile becomes filled-in by wind emission. Because of the blue-to-red asymmetry of the different processes, the total profile shows a certain asymmetry as well. Finally, for very large mass-loss rates, the first integral on the blue side vanishes completely, whereas the emission on the blue side (2nd integral) becomes fairly similar to the combined contribution from both integrals on the red one. Consequently, an almost symmetric emission profile is obtained, as displayed on the title page of this manual.

In this case, the H$_\alpha$-emission can be readily understood, without any insight into the theory of radiative transfer. Basically, we see photons which have been emitted within a large wind volume, due to the decay of excited electrons from level 3 to level 2. Since these are additional photons (compared to the stellar continuum), the profile inevitably needs to be in emission. To understand the specific *shape* of the profile, however, one has at least to account for the impact of the Doppler-effect.

8   Experimental procedure

All required data and parameters can be found in the appendix!

8.1   UV-analysis

Analyze the Nv and the Civ line for two stars from the sample of Galactic O-stars as tabulated in the appendix. The supervisor will tell you which stars should be considered.

The programmes, data and output-files (which will be created by you) can be found in the directory uv. The IDL[17]-routine required for the line-fits (don't worry, everything has been programmed in such a way that you don't need any knowledge regarding this programming/data visualization package) is called uv.pro.

8.1.1   Parameter study

In order to develop a "feeling" how the profiles react on the variation of the different parameters,

- v_∞, β, k_o, α

you should vary, in a first series of tests, one parameter while keeping the remaining three fixed. Study carefully the corresponding reactions and try to understand them, so that you can successfully fit the actual observations later on. To this end, perform the following tests, with basic parameters

- $v_\infty = 2000$ km/s

- $\beta = 1$

- $\log k_o = 0$

- $\alpha = 0$

To start the simulation, run the command (in the IDL-shell)

```
uv,'testname','000'
```

For testname, use a conclusive name which allows for an easy identification of your results. (The quotation marks need to be provided as well). The identification '000' tells the programme *not* to compare with any observation.

The further procedure (input, output) is almost self-explanatory, and questions will be answered by the supervisor. In total, carry out the following test series:

- test1: $v_\infty = 500, 2000, 4000$ km/s

- test2: $\beta = 0.5, 0.8, 1., 2.$

- test3: $\log k_o = -2, -1, 0, 1$

- test4: $\alpha = 2., 0., -3.$

Remember to keep the other parameters at their "nominal" value from above. When you are finished with one series, respond, after the request HARDCOPY?, with the answer 2 (corresponding to test(NV + CIV), and follow the further instructions by the programme. Your output will be written into subdirectory catout, with obvious file-names, following the identifier (testname) provided by you. Don't forget to print all output files (postscript) at the end of this test series.

---

[17]Interactive Data Language

8.1.2   Analysis of the Galactic sample

Use the Nv and Civ lines from two stars (see above) to derive the terminal velocity, v_∞, and the wind-/line-strength parameters β, k_o, α.

[The parameters for the remaining stars will be provided by the supervisor at the end of the 2nd afternoon. Note that for the stars HD 93128, HD 18409, HD 193514 and α Cam there are no spectra available in our catalogue. The v_∞ values provided in Table 1 have been estimated from the spectral type (HD 93128, HD 18409), or derived from independent UV spectroscopy (HD 193514, α Cam).]

To run the fit-routine, use

```
uv,'star_name','xxx'
```

where 'star_name' is the name of the star and 'xxx' (again with quotation marks) the file-number of the corresponding observations (see Table 1). After you have obtained (hopefully) a satisfactory fit, respond, after the request HARDCOPY?, this time with the answer 1 (yes). The output for both lines will be created under catout/star_name_uv.ps. Don't forget to record the final parameters.

Hint: At first, determine v_∞. Use $\log k_o = 1$ and $\alpha = 0$ as initial values. Only after determining v_∞ from both profiles, you should begin with the variation of the other parameters. Note: for unsaturated profiles, v_∞, k_o and α need to be fitted in parallel.

Remark: Even when trying very hard, some profiles cannot be fitted in the blue region where the profile begins to rise towards the emission peak. In that case, try to derive limiting values and concentrate on the outer part of the wind. The origin of this problem will be discussed during the 2nd afternoon.

8.1.3   Coarse estimate of the expected column density

To avoid errors arising from the conversion of units etc., everybody is well advised to *estimate* the expected magnitude of a certain result when the corresponding relation is difficult to evaluate. Thus, provide a rough estimate on the expected order of magnitude of the column density according to Eq. 37. Note that the integral should be of order unity, since one integrates over a normalized quantity. Check your result with your supervisor! (Otherwise you might run into time consuming problems during your elaboration).

8.2 H_α-analysis

Determine the mass-loss rates and the velocity field exponents, β, for the same two stars from the sample. The working directory is now halpha. The output files (created again via HARDCOPY = 1) will be saved in sub-directory catout, with file name filename_ha.ps. The IDL fitting routine is ha.pro, and needs to be run as

```
ha,'filename',vsini=x
```

(vsini is the projected rotational velocity[18], see Table 1) or

```
ha,'filename',vsini=x,vrad=y,
```

---

[18]the reason why to account here for the rotational velocity while neglecting this in the UV profile fits will be discussed during the lab.

respectively, if there is an explicit value for the radial velocity, `vrad`, provided in Table 1. `filename` is the identifier of the observed H_α-spectrum, see Table 1. The routine will ask you for stellar parameters and v_∞ (from experiment 1) before you can proceed with fitting $\dot{M}$ and β.

8.2.1 Variation of parameters

Before fitting H_α of the first star, "play" with the two fit parameters to become familiar with the response of the theoretical profile. For this test series, use the first object as a standard, and investigate the following topics.

1. By varying $\dot{M}$, simulate a sequence of profiles, which

   - display a purely photospheric profile,
   - a profile where the photospheric one is slightly filled-in by wind emission,
   - a profile with weak emission and
   - a profile for a very large mass-loss rate, extending from v_∞ to $-v_\infty$ (rest-wavelength of $H_\alpha \approx 6562.8$ Å).

2. investigate the reaction on β, for the intermediate mass-loss rate (weak emission), for $\beta = 0.7, 1.0, 1.3$ and 2.0. Use `overplot` to plot all simulations into one figure, to enable an easy comparison.

After each finalized simulation, rename the created `*.ps` file in directory `catout`, since this will be overwritten by the following "fit". After these tests, print all figures.

8.2.2 Determination of $\dot{M}$ and β

Now, fit the synthetic profiles to the observations, and determine $\dot{M}$ and β. For the first object, show that the actual measurement quantity is Q (Sect. 5.3 and 7.2). How can this be obtained?

Don't forget to record the derived values, and print all figures!

Remark: Also here, for some of the profiles the blue part cannot be fitted in a satisfying way. This is due to an approximate description of an overlapping "line-blend" from HeII, and problems related to wind clumping (Sect. 10). In this case, concentrate on the fit to the red wing of the profile.

9 Elaboration

Your elaboration can be written in German!

9.1 Questions related to theory

1. Answer the 11 questions integrated into Sects. 1 to 7.

2. Which assumption has been implicitly made in the derivation of the WLR? (Hint: Which dependence of $\dot{M}$ has been suppressed in the scaling relations?)

3. What is the *dominating* error source when deriving the stellar radius from a given WLR?

9.2 Line diagnostics

1. Discuss the results from your parameter study of UV lines, and try to explain the response of the synthetic profiles on the variations of the individual parameters.

2. Derive, from your results and the data provided for the remaining stars, the column densities, N^{col} (or corresponding limits), as well as the mean ionization fractions, $\overline{X}_k$, for Nv and Civ in the velocity interval $[0.2; 1]$ (for atomic data, see appendix). (Hint: Since $\overline{X}_k$ is a *fraction*, it cannot be larger than unity. Minimum values for our sample are of the order of 10^{-4}).

3. Plot your results for $\overline{X}_k$ (logarithmically!, since otherwise nothing will be seen), as a function of T_{eff} and $\log L/L_{\odot}$, respectively, and separately for Nv and Civ. Discuss possible trends.

4. Compare the derived β values from the UV and the H_{α} analysis, and discuss possible reasons for the discrepancy.

5. Discuss your results regarding Q as the actual measurement quantity.

9.3 WLR for Galactic supergiants

1. Plot the modified wind-momentum rates, $\log(\dot{M}v_{\infty}(R_*/R_{\odot})^{\frac{1}{2}})$, as a function of $\log(L/L_{\odot})$. Discriminate supergiants from stars of other luminosity classes by different symbols.

2. Determine the WLR for Galactic supergiants, by means of a least-squares fit. What is the position of the other luminosity-class stars, compared to this relation. What could be the reason for this difference? (Remember: theory does not predict such a difference).

3. Use the WLR derived by you to estimate the radius of the LMC supergiant Melnick 42 in the LMC (see title page and Fig. 11). Which assumption needs to be made by doing so? (Hint: remember the various dependencies of the WLR).

   Parameters of Mk 42: $T_{\text{eff}} = 50,500$ K, $v_{\infty} = 3000$ km/s, $Q = 2.64 \cdot 10^{-7} M_{\odot}$/yr (remember: $Q = \dot{M}/(R_*/R_{\odot})^{3/2}$).

4. From the radius obtained, estimate the distance to the LMC, by using the following relation between stellar radius and absolute visual magnitude (derived from the *bolometric correction* for hot stars, see Martins et al. 2005, A&A 436, 1049),

$$\log(R_*/R_{\odot}) = 2.96 - 0.2M_V - 0.64\log(T_{\text{eff}}/\text{K}) \tag{47}$$

What is the estimated *distance modulus*, when the visual magnitude of Mk 42 is $V = 12.64^{\mathrm{m}}$ and the reddening is $A_V = 1.24^{\mathrm{m}}$? Express the estimated distance to the LMC in kpc, and compare with literature values. Discuss the difference, if there is any.

Add all fits and results from your parameter studies to your elaboration, including reasonable figure captions.

10   Final comments

In this lab we have (hopefully) shown how the spectra of hot stars can be used to infer essential information about their winds, and derived an important relation – the WLR – which enables (i) an alternative method to determine extragalactic distances on intermediate scales and (ii) allows for simple tests of the theory of line-driven winds.

As already stated, reality is much more complex compared to the simplifications made in this manual. By means of more elaborate approaches, a number of exciting results regarding line-driven winds have been obtained during recent years, by members of our and other working groups. The present picture can be briefly summarized as follows:

- for the majority of analyzed objects, the theory of line-driven winds is in very good agreement with observations, i.e., radiative line driving has been established as the *dominating* accelerating mechanism in stellar winds.

- under certain circumstances, the influence of rotation[19] and magnetic fields[20] needs to be accounted for. Corresponding theories have been developed, and are in the test phase meanwhile.

- Two major problems have been identified, which are the objective of present work in our group and elsewhere:

  1. The "weak wind problem": Particularly for O-dwarfs of late spectral type (around O9V), the derived mass-loss rates are often much lower than predicted by theory, by factors of 10 to 100. This fact is a real challenge for the theory.
  2. Wind-clumping: Numerous observational facts indicate that the winds are not homogeneous, but consist of clumps with over-densities (compared to a smooth wind) of factors between 10 and 100, and an almost void inter-clump medium. The origin for such an inhomogeneous structure is conventionally attributed to a strong instability inherent to radiative driving, which might compress the wind material into clumps. The most important effect of such clumping concerns the wind diagnostics. (i) Resonance and recombination lines react differently on wind-clumping. (ii) Most mass-loss rates derived so far from recombination lines[21] turn out to be too large, by factors of 3 to 5. Consequences of wind clumping on the WLR and on the wind physics itself are in the focus of present day's activities of hot star wind research!

---

[19]a significant fraction of hot stars are very fast rotators, with rotation speeds up to several 100 km/s.

[20]even weak fields (below the present detection limit of 50 to 100 Gauss) can have a severe impact, when the mass-loss rate is low.

[21]including those quoted in this manual.

11 Appendix: Tables and data

11.1 A sample of Galactic O-stars

Table 1: Parameters of our sample of Galactic O-stars. T_{eff} in kK, R_* in $R_\odot$, v_{rad}, $v \sin i$, v_∞ in km/s, $\dot{M}$ in $10^{-6} M_\odot$/yr. "used" refers to the effective value of $v \sin i$, if this is different from the photospheric value (due to *differential* rotation). The values for the radial velocity, v_{rad} – if any – refer to arbitrary shifts of the observed profile and do not relate to the actual values.

[1] File name of the observed H_α-profile, to be used in routine `ha`
[2] File number of the observed UV profile, to be used in routine `uv`
[3] Fit value from H_γ (photospheric and wind-contaminated).
[4] "True" value inclusive correction terms for wind effects and centrifugal forces.
[5] v_∞ estimated from spectral type

star	classif.	file[1]	no.[2]	T_{eff}	R_*	$\log g$[3]	$\log g$[4]	Y	v_{rad}	$v \sin i$	used	v_∞
HD 93128	O3 V ((f))	HD93128		52.0	10.	4.00	4.00	0.10	-10	100		3100[5]
HD 93250	O3 V ((f))	HD93250	088	50.5	18.	3.95	4.00	0.10		100		
HD 93129A	O3 I f*	HD93129A	079	50.5	20.	3.80	3.95	0.10		130		
HD 303308	O3 V ((f))	HD303308	195	48.0	12.	4.05	4.10	0.10		100		
ζ Pup	O4 I (f)	HD66811	061	42.0	19.	3.50	3.60	0.12		220		
HD 15558	O5 III (f)	HD15558	012	48.0	21.8	3.80	3.85	0.08	-75	120		
HD 15629	O5 V ((f))	HD15629	014	47.0	14.2	3.90	3.90	0.08	-75	90		
HD 14947	O5 I f$^+$	HD14947	010	43.5	16.1	3.45	3.50	0.18	-25	140		
λ Cep	O6 I(n) fp	HD210839	187	38.0	19.	3.60	3.65	0.10		210		
HD 190864	O6.5 III (f)	HD190864	171	41.0	14.1	3.55	3.55	0.20		105		
HD 217086	O7 V n	HD217086	190	40.0	10.3	3.60	3.75	0.20		375	290	
HD 192639	O7 Ib (f)	HD192639	174	38.5	19.5	3.40	3.45	0.25		125		
HD 193514	O7 Ib (f)	HD193514	177	38.0	19.8	3.40	3.45	0.14		105		2200
HD 203064	O7.5 III:n ((f))	HD203064	181	37.5	14.1	3.50	3.65	0.14		315	190	
ξ Per	O7.5 III (n)((f))	HD24912	019	36.0	25.5	3.30	3.40	0.22	55	250	100	
HD 13268	ON8 V	HD13268	006	35.0	11.7	3.30	3.50	0.25	-120	320	250	
HD 191423	O9 III : n*	HD191423	173	34.0	13.	3.40	3.70	0.25	-70	450	300	
HD 207198	O9 Ib-II	HD207198	183	34.0	15.1	3.30	3.30	0.14		80		
HD 210809	O9 Iab	HD210809	186	33.0	21.7	3.10	3.15	0.14		100		
ζ Oph	O9 III	HD149757	124	32.5	12.9	3.70	3.85	0.19		400	300	
HD 209975	O9.5 Ib	HD209975	185	32.5	17.2	3.20	3.20	0.10	-30	100		
HD 18409	O9.7 Ib	HD18409		31.5	16.1	3.10	3.15	0.14	-55	160	80	1750[5]
α Cam	O9.5 Ia	HD30614	029	30.0	29.	2.95	3.00	0.20		80		1550

11.2   Some data required during this lab

$T_{\mathrm{eff}\odot} = 5777\,\mathrm{K}$
$R_\odot = 6.96 \cdot 10^{10}\,\mathrm{cm}$
one year $= 3.1558 \cdot 10^7\,\mathrm{s}$

$\pi\mathrm{e}^2/(m_\mathrm{e}c) = 0.02654$ in cgs
$m_\mathrm{H} = 1.673 \cdot 10^{-24}\,\mathrm{g}$

Data for the Nv line (blue component, solar abundance)

$f_{lu} = 0.157$
$\lambda_{lu} = 1238.8\,\text{Å}$
$\log A_N = -4.22$

Data for the Civ line (blue component, solar abundance)

$f_{lu} = 0.1908$
$\lambda_{lu} = 1548.2\,\text{Å}$
$\log A_C = -3.61$